

Bose-Einstein Condensation versus Dicke-Hepp-Lieb Transition in an Optical Cavity

Francesco Piazza^{1,*}, Philipp Strack², and Wilhelm Zwerger¹

¹*Physik Department, Technische Universität München, 85747 Garching, Germany and*

²*Department of Physics, Harvard University, Cambridge MA 02138*

We provide an exact solution for the interplay between Bose-Einstein condensation and the Dicke-Hepp-Lieb self-organization transition of an ideal Bose gas trapped inside a single-mode optical cavity and subject to a transverse laser drive. Based on an effective action approach, we determine the full phase diagram at arbitrary temperature, which features a bi-critical point where the transitions cross. We calculate the dynamically generated band structure of the atoms and the associated suppression of the critical temperature for Bose-Einstein condensation in the phase with a spontaneous periodic density modulation. Moreover, we determine the evolution of the polariton spectrum due to the coupling of the cavity photons and the atomic field near the self-organization transition, which is quite different above or below the Bose-Einstein condensation temperature. At low temperatures, the critical value of the Dicke-Hepp-Lieb transition decreases with temperature and thus thermal fluctuations can enhance the tendency to a periodic arrangement of the atoms.

I. INTRODUCTION

The study of light-matter interactions at the level of single atoms and photons is a major subject in atomic and molecular physics. The strong atom-field coupling which is achievable in high quality cavities has allowed to generate entangled states between light and atoms [1] or to directly observe the appearance or disappearance of single photons [2]. The backaction of a single atom onto a cavity can shift its frequency appreciably, as evidenced by a finite vacuum Rabi splitting [3]. New and interesting phenomena at the interface between cavity-QED and many-body physics arise in a situation where the cavity contains a finite density of atoms which may undergo either thermal or quantum phase transitions on their own. A simple case in question is a cavity filled with an ultracold gas of bosons and subject to a transverse drive due to the coherent field of a pump laser. As predicted by Domokos and Ritsch [4], the backaction of the atoms on the light in the presence of a transverse driving can lead to the formation of a spontaneous density modulation of the atoms. The lattice spacing of the resulting crystalline order is set by the cavity mode wavelength, thus optimizing the Bragg scattering of the laser photons into the cavity mode. Simultaneously, the cavity mode itself acquires a finite expectation value which leads to a change of the spectrum of polaritons in the cavity. This transition to a spatially ordered state of atoms in a cavity has been observed experimentally first with thermal atoms [5] and - more recently - with a Bose-Einstein condensate [6–9]. These experiments are conceptually related to the already observed non-steady-state effects like superradiant Rayleigh scattering [10–12] and collective recoil lasing [12, 13].

A standard theoretical description of the transition to a self-ordered, periodic arrangement of the atoms in a transversely driven cavity assumes that the atomic wave vectors can be truncated to just two, namely $\mathbf{k} = 0$ and the cavity mode wave vector $\mathbf{k} = \mathbf{k}_0$. Within such a two-mode approximation, the problem is reduced to an effective Dicke model [14]

where a large spin of length $J = N/2$ is linearly coupled to the quadrature $\sim (\hat{a}^\dagger + \hat{a})$ of the cavity field. Surprisingly, to date [15], it has remained unclear how the simplified description within a generalized Dicke model [16–29] or the semiclassical treatment of the atomic field [30, 31] is connected to the actual many-body situation in which the Bose gas can either be Bose-condensed or in a thermal state at higher temperatures. In particular, a study of whether and how the properties of the self-organization transition change between the BEC limit studied in the ETH experiments [6] and the earlier ones in a thermal gas at MIT [5] has been lacking.

A. Key results

Our aim in the present paper is to develop a comprehensive description of the backaction between atoms and light field in a driven cavity, which properly describes the interplay between the Dicke-Hepp-Lieb (DHL) type transition to a state with a periodic density modulation of the atoms and the transition to a phase coherent Bose-Einstein condensate. As will be shown below, the Dicke model provides a correct description of the transition to spatial order of the atoms only in the special case of an ideal gas of bosons at zero temperature. Indeed, the presence of a continuum of atomic momenta at any finite temperature or, even at $T = 0$, if repulsive interactions are appreciable, precludes a truncation of the problem to just two momenta $\mathbf{k} = 0$ and the cavity mode wave vector $\mathbf{k} = \mathbf{k}_0$.

To address the full quantum many-body problem, we develop an effective action approach that allows to derive the detailed form of the cavity spectrum and the dynamically generated bandstructure for the atoms in a fully quantum mechanical fashion, without resorting to any semi-classical approximations or truncating the Hilbert space to a simplified two-state Dicke model.

Apart from the quite different symmetry breakings involved (as we discuss in more detail below), the DHL and BEC transitions are fundamentally distinct also in the sense that the former is caused by an external driving in an open system while the transition to a BEC is due to the standard competition between energy and entropy in an equilibrium situation. De-

* francesco.piazza@ph.tum.de

spite these differences, it will be shown that an effective action approach which is based on the assumption of a steady thermal equilibrium state of the coupled atom-field configuration in a cavity provides a unified description of both transitions and even captures some of the non-equilibrium features of the DHL transition. Restricting to the case of non-interacting Bosons in a first step, our main results are:

i) A quantitative phase diagram for the driven cavity problem at arbitrary temperatures. It contains four different phases which are degenerate at a special bi-critical point. The state of the atoms in these phases are either a thermal or a BEC phase which can both be either homogeneous or spatially ordered at a wave vector set by the cavity mode and multiples thereof.

ii) A calculation of the dynamical band structure arising for the atoms due to the backaction from the cavity field. With increasing depth of the temperature dependent lattice, the BEC transition temperature is strongly suppressed.

iii) A detailed description of the cavity spectral function associated with polaritonic excitations which are thermally broadened and sensitive to the presence or absence of the BEC. In particular, at finite temperature, the divergence of the emitted light intensity close to the self-organization transition exhibits a thermal behavior.

B. Outline of paper

In Sec. II, we recapitulate the standard model Hamiltonian and cavity set-up. We also discuss the underlying symmetries and the mapping to the Dicke model, to make contact with earlier studies. In Sec. III, we express the partition function of the coupled atom-cavity set-up in terms of an exact, imaginary time path integral. We derive an effective action, nonlocal in space and time, which contains the full backaction between the atoms and the cavity field. The self-consistent solution of the resulting saddle-point equations allows to determine the full phase diagram, the dynamical band structure of the atoms and the behavior of the superfluid condensate and cavity field as function of temperature and atom-cavity coupling. The results are discussed in detail in Sec. IV. In Sec. V, we analyze in detail the cavity spectrum, in particular its singular behavior near the transition to self-organization and also across the Bose-Einstein condensation temperature. In Sec. VI, we discuss the scaling properties of the effective photon action in the limit of large atom numbers. It is shown that the mean-field solution becomes exact in this limit. We conclude in Sec. VII with some open problems and a critical discussion of the advantages and limitations of using an effective equilibrium formalism for a description of a dissipative open system.

II. MODEL

We consider N atoms with two internal electronic levels trapped inside a transversally driven cavity. The atoms are illuminated by a pump laser and are also coupled with a single cavity mode. In terms of the quantized field operators $\hat{\psi}_{g/e}$ for the atoms in the internal ground or excited state and the

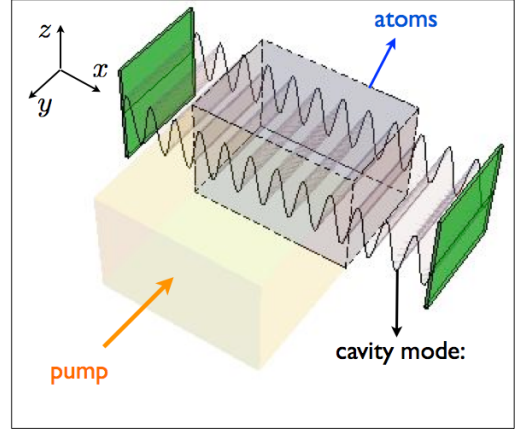


FIG. 1. The atoms, confined in a three-dimensional box (in blue), are interacting with a single cavity mode modulated along the x direction, and illuminated by the pump laser propagating transversally with respect to the cavity axis.

annihilation operator \hat{a} for a cavity photon, the complete atom plus driven cavity Hamiltonian reads [32]

$$\hat{H} = \hat{H}_a + \hat{H}_c + \hat{H}_{a/c} + \hat{H}_{a/p}, \quad (1)$$

where

$$\begin{aligned} \hat{H}_a &= \int d\mathbf{r} \left[\hat{\psi}_g^\dagger(\mathbf{r}) \left(-\frac{\nabla^2}{2m} \right) \hat{\psi}_g(\mathbf{r}) + \hat{\psi}_e^\dagger(\mathbf{r}) \left(-\frac{\nabla^2}{2m} - \Delta_a \right) \hat{\psi}_e(\mathbf{r}) \right] \\ \hat{H}_c &= -\Delta_c \hat{a}^\dagger \hat{a} \\ \hat{H}_{a/c} &= -i g_0 \int d\mathbf{r} \hat{\psi}_g^\dagger(\mathbf{r}) \eta_c(\mathbf{r}) \hat{a}^\dagger \hat{\psi}_e(\mathbf{r}) + \text{h.c} \\ \hat{H}_{a/p} &= -i \Omega \int d\mathbf{r} \hat{\psi}_g^\dagger(\mathbf{r}) \eta_p(\mathbf{r}) \hat{\psi}_e(\mathbf{r}) + \text{h.c} \end{aligned}$$

in the frame rotating with the pump frequency ω_p . Here, $\Delta_a = \omega_p - \omega_e$ and $\Delta_c = \omega_p - \omega_c$ are the detunings between the pump and the atomic resonance, and the pump and the cavity mode, respectively (we set $\hbar = 1$ except in some final results). Moreover, m is the atomic mass, g_0 is the single-photon Rabi coupling between the atom and the cavity and Ω is the pump Rabi frequency. The functions $\eta_c(\mathbf{r})$, $\eta_p(\mathbf{r})$ contain the spatial form of the cavity and pump modes, respectively. The main approximations involved are i) dipole and rotating wave approximation for the light-matter coupling, ii) neglect of the short-range interaction between atoms iii) neglect of spontaneous emission from the excited state and of cavity loss processes through the mirrors.

A. Symmetry breaking at the Dicke-Hepp-Lieb and the BEC transition

In order to discuss which symmetries are broken at either the DHL-transition where the atoms acquire a non-vanishing density modulation and the standard BEC transition, we need to fix the shape of the cavity and pump mode profiles. It is

also convenient to adiabatically eliminate the excited, atomic state. The latter step is justified in the limit of large atom-pump detunings Δ_a and is discussed in more detail below. The resulting, simplified effective Hamiltonian of the cavity-Bose gas system that only involves the atomic ground state is [32]

$$\begin{aligned}\hat{H}_{\text{eff},a} &= \int d\mathbf{r} \hat{\psi}_g^\dagger(\mathbf{r}) \left\{ -\frac{\nabla^2}{2m} + \frac{\Omega^2}{\Delta_a} \right\} \hat{\psi}_g(\mathbf{r}) \\ \hat{H}_{\text{eff},c} &= -\Delta_c \hat{a}^\dagger \hat{a} \\ \hat{H}_{\text{eff},a/c} &= \int d\mathbf{r} \hat{\psi}_g^\dagger(\mathbf{r}) \left\{ \frac{(g_0 \eta_c(\mathbf{r}))^2}{\Delta_a} \hat{a}^\dagger \hat{a} + \frac{\Omega g_0 \eta_c(\mathbf{r})}{\Delta_a} (\hat{a} + \hat{a}^\dagger) \right\} \hat{\psi}_g(\mathbf{r}),\end{aligned}\quad (2)$$

where we have used $\eta_p(\mathbf{r}) = 1$, i.e. the spatial structure of the pump laser is neglected in accordance with the simplified geometry illustrated in Fig. 1. We assume the atoms to be confined in a cavity with volume V and a cavity mode which extends all over the cloud with spatial modulation only along the x direction such that

$$\eta_c(\mathbf{r}) = \cos(\mathbf{k}_0 \cdot \mathbf{r}) \quad , \quad \mathbf{k}_0 = (k_0, 0, 0). \quad (3)$$

The Hamiltonian in Eq. (2) is invariant under a simultaneous parity transformation \mathcal{P} of the photons ($\mathcal{P} : \hat{a} \rightarrow -\hat{a}$) and a discrete, translational symmetry operation \mathcal{R} , which shifts the spatial coordinate of the atoms by odd multiples of the inverse cavity wave vector along the cavity axis direction x as $\mathcal{R} : \mathbf{r}_x \rightarrow \mathbf{r}_x \pm \pi/k_0$. In terms of a modulated atomic density operator $\hat{\rho}_{\mathbf{k}_0} = \int d\mathbf{r} \hat{\psi}_g^\dagger(\mathbf{r}) \hat{\psi}_g(\mathbf{r}) \cos(\mathbf{k}_0 \cdot \mathbf{r})$, the last term in Eq. (2), which is responsible for the self-organization transition, can be written as $\Omega g_0 \hat{\rho}_{\mathbf{k}_0} (\hat{a} + \hat{a}^\dagger)$. The symmetry operations \mathcal{R} and \mathcal{P} act on that term effectively as a Z_2

$$Z_2 : \hat{\rho}_{\mathbf{k}_0} \rightarrow -\hat{\rho}_{\mathbf{k}_0}, \quad \hat{a} \rightarrow -\hat{a}, \quad \hat{a}^\dagger \rightarrow -\hat{a}^\dagger, \quad (4)$$

leaving the Hamiltonian invariant under the product \mathcal{RP} . At the self-organization transition, the cavity develops a coherent field $\pm(\hat{a} + \hat{a}^\dagger) \neq 0$ into one of the two parity states available. In contrast to the BEC transition, there is no continuous symmetry breaking, however, associated with the appearance of condensate in the cavity field. Indeed the phase of the coherent state is locked to the phase of the pump laser with an extensive coupling energy E_J^{th} , see Eq. (27) below.

Simultaneous with the appearance of a non-vanishing average cavity field, the atoms spontaneously arrange into one of the two available checkerboard patterns $\pm\langle\hat{\rho}_{\mathbf{k}_0}\rangle$. As will be discussed in Section V, there is a soft mode associated with the formation of the lattice structure in the atoms, whose frequency vanishes at the transition. Due to the discrete symmetry breaking, this is not a Goldstone mode, however, and - moreover - it is overdamped near the transition (see Eq. (45) below).

The second symmetry of Eq. (2) is the continuous $U(1)$ -symmetry associated with the conservation of the number of atoms. Eq. (2) is invariant under the global shift

$$U(1) : \theta(\mathbf{r}) \rightarrow \theta(\mathbf{r}) + c, \quad (5)$$

by a constant, real-valued number c of the phase of the atomic field operator $\hat{\psi}_g(\mathbf{r}) = \rho(\mathbf{r})e^{i\theta(\mathbf{r})}$. While this symmetry is not

spontaneously broken in the relevant case with a fixed number of atoms in the cavity, the atomic field still exhibits off-diagonal long range order below the BEC transition temperature. The associated non-vanishing rigidity energy $\sim (\nabla \theta(\mathbf{r}))^2$ with respect to small gradients of the phase implies the existence of a proper Goldstone mode for the BEC transition [33]. In the non-interacting gas, its dispersion is that of free particles $\epsilon(\mathbf{k}) = \hbar^2 \mathbf{k}^2 / 2m$, while for any finite, repulsive interaction it is a linearly dispersing Bogoliubov sound mode. The change from a Goldstone mode with quadratic to one with a linear dispersion upon introducing interactions is due to the finite compressibility in the latter case, which entails a formal relativistic invariance in the quantum hydrodynamic description of the broken symmetry phase [33].

B. Hilbert space truncation to Z_2 Dicke model

As mentioned in the Introduction and discussed in detail in Refs. 6 and 20, one can map Eq. (2) to the Dicke model upon truncating the Hilbert space of the atoms to containing two momentum states only. Within such a two-mode approximation, the problem is reduced to an effective Dicke Hamiltonian [14]

$$\hat{H} = \delta_c \hat{a}^\dagger \hat{a} + E_R \hat{J}_z + \frac{\lambda}{\sqrt{2N}} (\hat{a}^\dagger + \hat{a}) (\hat{J}_+ + \hat{J}_-), \quad (6)$$

where a large spin of length $J = N/2$ is linearly coupled to the quadrature of the cavity field. The collective angular momentum operators in the two-mode Hilbert space of the N atoms are: $\hat{J}_z = \frac{1}{2} \sum_{j=1}^N (|\mathbf{k}_0\rangle_j \langle \mathbf{k}_0| - |\mathbf{0}\rangle_j \langle \mathbf{0}|)$, $\hat{J}_+ = \sum_{j=1}^N |\mathbf{k}_0\rangle_j \langle \mathbf{0}|$ and $\hat{J}_- = \sum_{j=1}^N |\mathbf{0}\rangle_j \langle \mathbf{k}_0|$. The effective magnetic field which couples to the spin polarization \hat{J}_z is determined by the recoil energy $E_R = \epsilon(\mathbf{k}_0) = \hbar^2 \mathbf{k}_0^2 / (2m)$ of a single atom at the wave vector \mathbf{k}_0 set by the cavity field. The Rabi coupling λ , the effective detuning of the cavity mode with respect to the atomic resonance δ_c , and the single-atom dispersive shift u_0

$$\lambda = \frac{\Omega g_0}{\Delta_a} \sqrt{N}, \quad \delta_c = -\Delta_c + \frac{1}{2} u_0, \quad u_0 = \frac{g_0^2}{\Delta_a} N \quad (7)$$

are all defined so that they approach finite values $\propto \sqrt{n}$ in the thermodynamic limit (TL): $N, V \rightarrow \infty$, $N/V = n = \text{const.}$ Indeed, the bare coupling g_0 decreases like $1/\sqrt{V}$ when the cavity volume is increased. Typical order of magnitudes for these couplings in quantum-optical experiments are recoil energies E_R in the kHz regime and pump-cavity detunings Δ_c in the MHz regimes, while temperatures T are in the micro-Kelvin to nano-Kelvin regime [15].

We note that in the effective Hamiltonian (6) the system volume V does not play any role once we know that the effective parameters are intensive quantities. In the Dicke model only the number of two-level atoms N enters and the TL is simply $N \rightarrow \infty$. In this limit, a standard Holstein-Primakoff expansion $J_- = \sqrt{N - \hat{b}^\dagger \hat{b}} \hat{b} \simeq \sqrt{N} \hat{b}$ of the angular momentum operators reduces the Dicke model to a rather simple

Hamiltonian of two harmonic oscillators with a linear coupling $\sim (\hat{a}^\dagger + \hat{a})(\hat{b}^\dagger + \hat{b})$, which leads to a crossing of the two eigenfrequencies [34].

Eq. (6) maps the Bose gas in a cavity to a zero-dimensional problem of a single, large- N spin coupled to a single harmonic oscillator. The two degenerate density patterns of the atoms discussed above correspond to the two degenerate orientations of a large Ising spin with length proportional to the number of atoms N . Note that Eq. (6) contains counter-rotating terms and is invariant under a discrete Z_2 transformation: $\hat{J}_+ \rightarrow -\hat{J}_+$, $\hat{J}_- \rightarrow -\hat{J}_-$, $\hat{a} \rightarrow -\hat{a}$, $\hat{a}^\dagger \rightarrow -\hat{a}^\dagger$. Without counter-rotating terms the so-called $U(1)$ Dicke model has an additional global $U(1)$ symmetry [34, 35] which is not to be confused with the $U(1)$ of the atoms introduced in Eq. (5).

The Dicke model has a number of important properties which - later on in our paper - we will compare with the results for the full problem which does not rely on the two-state truncation:

(a) *Exact solvability*: The Dicke model [14] is a zero-dimensional model and can be solved exactly at arbitrary temperatures in the TL $N \rightarrow \infty$ [36, 37]. It exhibits the Dicke-Hepp-Lieb (DHL) transition to a superradiant state, in which the ground state has a finite occupation of the photon mode combined with a finite atomic polarization.

(b) *Quantum bifurcation rather than phase transition*: The DHL transition is a quantum bifurcation in a zero-dimensional system. As a result one may define a critical exponent $z\nu = 1/2$ [38] from the vanishing of the soft mode frequency but the exponents z and ν have no separate meaning because there is no divergent correlation length here.

(c) *Finite temperature phase boundary*: At finite temperature, the critical spin-photon coupling turns out to be [36, 37]

$$\lambda_D^2(T) = \frac{E_R \delta_c}{2 \tanh(E_R/2k_B T)}, \quad (8)$$

As will be shown in Sec. IV B, the Dicke model gives the correct value for the critical coupling both at very low and at high temperatures $k_B T \gg E_R$. However, within the full theory, there is an intermediate regime, at which thermal fluctuations in fact favor a spatially ordered pattern of the atoms. This is not captured within the Dicke model expression for the critical coupling Eq. (8), which is instead a monotonously growing function of temperature T . Moreover, the temperature dependence of the number of condensed atoms, also not included in the Dicke model, affects the critical coupling in a non-trivial way.

III. EFFECTIVE ACTION APPROACH

In this section, we derive a Landau-Ginzburg-Wilson type effective action for the coupled order parameters which characterize both the DHL- and the BEC transition. Beyond the complex cavity field, the order parameter of the atoms is a spinor with an infinite number of terms associated with Fourier components of the condensate at wave vectors which are an arbitrary multiple of \mathbf{k}_0 . The effective action is derived

by eliminating all other degrees of freedom from our problem, which can be conveniently done using the path-integral formalism. Starting with the time-independent Hamiltonian (1), the associated partition function can be expressed as a functional integral in the form

$$\mathcal{Z} = \int D(\psi_e^*, \psi_e) D(\psi_g^*, \psi_g) D(a^*, a) e^{-S[\psi_e^*, \psi_e, \psi_g^*, \psi_g, a^*, a]}.$$

We decompose the fields as

$$\psi_{g/e}(\mathbf{r}, \tau) = \frac{1}{\beta \sqrt{V}} \sum_{\mathbf{n}, \mathbf{k}} e^{-i\omega_n \tau + i\mathbf{k} \cdot \mathbf{r}} \psi_{g/e; \mathbf{n}\mathbf{k}}, \quad a(\tau) = \frac{1}{\beta} \sum_{\mathbf{n}} e^{-i\omega_n \tau} a_{\mathbf{n}}$$

into the Fourier components of the fluctuating atom and cavity field in imaginary time τ . Here $\omega_n = 2\pi n/\beta$ is a bosonic Matsubara frequency and $\beta = 1/(k_B T)$ the inverse temperature. The different contributions to the Hamiltonian (1) give rise to a corresponding sum of action terms

$$S[\psi_e^*, \psi_e, \psi_g^*, \psi_g, a^*, a] = S_a + S_c + S_{a/c} + S_{a/p}, \quad (9)$$

which read

$$\begin{aligned} S_a &= \frac{1}{\beta} \sum_{\mathbf{n}, \mathbf{k}} \psi_{e; \mathbf{n}\mathbf{k}}^* (-i\omega_n + \epsilon(\mathbf{k}) - \mu - \Delta_a) \psi_{e; \mathbf{n}\mathbf{k}} \\ &\quad + \frac{1}{\beta} \sum_{\mathbf{n}, \mathbf{k}} \psi_{g; \mathbf{n}\mathbf{k}}^* (-i\omega_n + \epsilon(\mathbf{k}) - \mu) \psi_{g; \mathbf{n}\mathbf{k}} \\ S_c &= \frac{1}{\beta} \sum_{\mathbf{n}, \mathbf{k}} a_{\mathbf{n}}^* (-i\omega_n - \Delta_c) a_{\mathbf{n}} \\ S_{a/c} &= \frac{ig_0}{2\beta^2} \sum_{\mathbf{n}, \mathbf{n}', \mathbf{k}} a_{\mathbf{n}-\mathbf{n}'}^* \psi_{g; \mathbf{n}'\mathbf{k}}^* (\psi_{e; \mathbf{n}\mathbf{k}-\mathbf{k}_0} + \psi_{e; \mathbf{n}\mathbf{k}+\mathbf{k}_0}) + \text{h.c.} \\ S_{a/p} &= \frac{i\Omega}{\beta} \sum_{\mathbf{n}, \mathbf{k}} \psi_{g; \mathbf{n}\mathbf{k}}^* \psi_{e; \mathbf{n}\mathbf{k}} + \text{h.c.}, \end{aligned}$$

where $\epsilon(\mathbf{k}) = \hbar^2 k^2/2m$ and $k = |\mathbf{k}|$.

As a first step, we integrate out the atomic field associated with the excited atomic level. Since the above action is quadratic in $\psi_{e; \mathbf{n}\mathbf{k}}$ plus source terms which are linear in $\psi_{e; \mathbf{n}\mathbf{k}}$, this elimination can be performed exactly by evaluating a Gaussian path-integral. For an arbitrary value of the detuning Δ_a , this introduces retardation effects with complicated effective couplings between the ground state atoms and the cavity field. The situation is considerably simplified in the experimentally relevant limit, where the detuning Δ_a , typically in the GHz regime, is much larger than the recoil energy and the atomic chemical potential, typically in the KHz regime. In this limit, the dynamics of the atoms in the excited states is irrelevant and the propagator $(-i\omega_n + \epsilon(\mathbf{k}) - \mu - \Delta_a)^{-1}$ for the excited atoms can be replaced by a constant $1/\Delta_a$. As a result, the excited atomic level is eliminated adiabatically, yielding

$$\begin{aligned} S'[\psi^*, \psi, a^*, a] &= \frac{1}{\beta^2} \sum_{\mathbf{n}, \mathbf{m}} \sum_{\mathbf{k} \in B} \Psi_{\mathbf{n}}^\dagger(\mathbf{k}) M_{\mathbf{n}, \mathbf{m}}(\mathbf{k}) \Psi_{\mathbf{m}}(\mathbf{k}) \\ &\quad + \frac{1}{\beta} \sum_{\mathbf{n}} (-i\omega_n - \Delta_c) |a_{\mathbf{n}}|^2. \quad (10) \end{aligned}$$

as an effective action for the ground state atoms plus the cavity field (in the following, we will drop the subscript g indicating the ground state atoms). Here, we employed a Nambu spinor representation

$$\Psi_n^T(\mathbf{k}) = \left(\dots \psi_{n,\mathbf{k}-2\mathbf{k}_0} \psi_{n,\mathbf{k}-\mathbf{k}_0} \psi_{n,\mathbf{k}} \psi_{n,\mathbf{k}+\mathbf{k}_0} \psi_{n,\mathbf{k}+2\mathbf{k}_0} \dots \right), \quad (11)$$

$$M_{n,m}(\mathbf{k}) = \begin{pmatrix} \dots & \dots & \dots & \dots & \dots \\ U_{n,m}/2 & \Lambda_{n,m}/2 & d_{n,m}(\mathbf{k}-\mathbf{k}_0) & \Lambda_{n,m}/2 & U_{n,m}/2 \\ 0 & U_{n,m}/2 & \Lambda_{n,m}/2 & d_{n,m}(\mathbf{k}) & \Lambda_{n,m}/2 \\ 0 & 0 & U_{n,m}/2 & \Lambda_{n,m}/2 & d_{n,m}(\mathbf{k}+\mathbf{k}_0) \\ \dots & \dots & \dots & \dots & \dots \end{pmatrix}. \quad (12)$$

is tridiagonal in Nambu space. Its diagonal elements

$$d_{n,m}(\mathbf{k}) = \delta_{n,m} G_0^{-1}(\omega_n; \mathbf{k}) + U_{n,m} \quad (13)$$

contain the inverse free boson propagator $G_0^{-1}(\omega_n; \mathbf{k}) = \beta(-i\omega_n + \epsilon(\mathbf{k}) - \mu)$, where μ is the chemical potential, which is shifted compared to its bare value by a contribution Ω^2/Δ_a due to the spatially homogeneous external drive. The propagator G_0 describes the intra-band dynamics of the atoms.

The second term

$$U_{n,m} = \frac{u_0}{2\beta N} \sum_{n_1} a_{n_1-n}^* a_{n_1-m}, \quad (14)$$

in Eq. (13) results from two photon processes where the atom absorbs a photon from the cavity and re-emits it into the latter. The corresponding effective vertex after elimination of the excited atomic level is illustrated by the upper Feynman diagram in Fig. 2. The atom-cavity coupling described by Eq. (14) is responsible for the dispersive shift of the cavity frequency induced by the atoms. More precisely, the shift is described by the diagonal part in Matsubara space $n = m$, while the off-diagonal part appears since the atoms can also induce fluctuations in the cavity and vice versa.

The off-diagonal elements of the matrix (12) describe the coupling between nearest and next-to-nearest neighbouring Bloch bands. The cavity field $a(\tau)$ only depends on the imaginary time variable τ since its spatial form is assumed to be always given by the stationary mode eigenfunction $\eta_c = \cos(\mathbf{k}_0 \cdot \mathbf{r})$. In line with most previous work, we keep the spatial structure of the photon mode unchanged by the presence of atoms or potential optomechanical couplings between the mirrors and intracavity photon field. This is justified as long as the dipole coupling g_0 is much smaller than the energy separation between the cavity modes. This ensures the effective zero-dimensionality of the problem and is crucial for the exact solvability of the model, as we discuss in Sec. VI. Including dispersive effects of the photons or self-consistently determining the cavity mode functions as a function of momentum sig-

for the atomic field, where every component of the spinor corresponds to a different Bloch band set by the cavity mode. The momentum sum in the action (10) is therefore restricted to the first Brillouin zone $\mathbf{k} \in B$, i. e. $\mathbf{k} = (-k_0/2 < k_x < k_0/2, -\infty < k_y < \infty, -\infty < k_z < \infty)$ in the simple geometry shown in Fig. 1. This spinor representation has the advantage that the matrix $M_{n,m}(\mathbf{k})$ in Eq. (10), containing the coupling between cavity and atoms, is diagonal in quasi-momentum \mathbf{k} . Its explicit form

nificantly complicates the analysis and we leave this to future work.

In the Feynman diagrams in momentum space, every cavity photon line thus has two possible momenta $\pm\mathbf{k}_0$, corresponding to photons travelling in opposite directions. This is why we have both super- and sub-diagonals in the matrix (12). For the same reason, the diagram for $U_{n,m}$ can contribute to both the intra-band coupling, when the atom absorbs a photon travelling in one direction and emits it in the same direction, and also to the next-to-nearest neighbor coupling, when the absorbed and emitted photons have opposite directions.

The presence of a transverse pump laser finally leads to a coupling

$$\Lambda_{n,m} = \frac{\lambda}{\sqrt{N}} (a_{m-n}^* + a_{n-m}), \quad (15)$$

between nearest neighboring bands. Note that the effective cavity-atom coupling is actually a two-photon process proportional to the amplitude of the pump laser Ω . So even for relatively small dipole matrix elements g_0 , by increasing the pump amplitude Ω , one can achieve sufficiently strong cou-

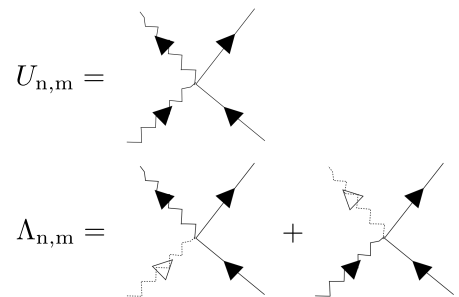


FIG. 2. Feynman diagrams for the effective scattering vertices between ground state atoms and photons. Solid lines correspond to atoms, zig-zag lines to cavity photons, dashed lines with empty arrows to pump photons.

plings λ to induce self-organization. The Feynman diagrams corresponding to Eq. (15) are shown in Fig. 2. In this effective vertex, the cavity photon is turned into a pump photon upon scattering with a ground state atom (or the other way around). This corresponds to an atom absorbing a photon from the pump and emitting it into the cavity (or the other way around).

In a second step towards an effective action which only contains the order parameters for both the DHL and BEC transition, we integrate out the fluctuations in the ground state atomic field $\Psi_n(\mathbf{k})$. In order to account for the possible occurrence of BEC, we separate out the condensate part in the standard form

$$\Psi_n(\mathbf{k}) = \beta\delta_{n,0}\delta_{\mathbf{k},0}\sqrt{N}\Phi_0 + \delta\Psi_n(\mathbf{k}), \quad (16)$$

where

$$\Phi_0 = \left(\dots \phi_{-2\mathbf{k}_0} \phi_{-\mathbf{k}_0} \phi_0 \phi_{\mathbf{k}_0} \phi_{2\mathbf{k}_0} \dots \right) \quad (17)$$

is the spinor describing the condensate wavefunction in Nambu space. It defines the number of atoms in the condensate $N_0 = N\Phi_0^\dagger\Phi_0$. At this point, it is important to realize that the BEC phase discussed here is of a multi-mode character in the regime where the cavity field acquires a non-vanishing average occupation. Indeed, as discussed before in the special case of zero temperature [24], a macroscopic occupation of momentum states of the atoms then appears not only in the $\mathbf{k} = 0$ mode but also in harmonics $\pm n\mathbf{k}_0$ of arbitrary order $n = 1, 2, \dots$ in the cavity wavevector \mathbf{k}_0 .

Since the scattering with a cavity photon cannot change the quasi-momentum of the atom but only its Bloch band, only the finite temperature can induce an occupation of a quasi-momentum different from zero. Therefore, as long as short-range interactions between the atoms are excluded, it is completely general to assume that the condensate spinor can only have quasi-momentum equal to zero, as done in Eq. (17). Moreover, in the absence of short-range interactions, the action (10) contains terms only up to second order in $\delta\Psi_n(\mathbf{k})$. The fluctuations of the ground state atoms can thus again be eliminated exactly by a Gaussian integral. By accounting properly for the non-standard terms which are linear in $\delta\Psi_n(\mathbf{k})$ and contain the condensate spinor Φ_0 , the resulting effective action is finally given by

$$S_{\text{eff}}[\Phi_0^\dagger, \Phi_0, a^*, a] = \frac{1}{\beta} \sum_n (-i\omega_n - \Delta_c) |a_n|^2 + \text{Tr} \ln(\mathbf{M}) + N\Phi_0^\dagger \mathbf{M}_{0,0}(\mathbf{0})\Phi_0 - N \sum_{n,m \neq 0} \Phi_0^\dagger \mathbf{M}_{0,n}(\mathbf{0}) \mathbf{M}_{n,m}^{-1}(\mathbf{0}) \mathbf{M}_{m,0}(\mathbf{0})\Phi_0. \quad (18)$$

In the tracelog term, the trace corresponds to $\sum_n \sum_{\mathbf{k} \in B} \text{tr}$, where tr indicates the trace in Nambu space. This term describes the contribution to the energy of the cavity photons originating from the coupling with thermal atoms only. The terms on the second line of Eq. (18) describe the contribution to the energy of the cavity photons due to the presence of condensed atoms. In particular, the last term describes processes where both condensed and thermal atoms are involved. We point out that here the summation is restricted

to $n, m \neq 0$. This restriction comes from requiring that the atomic fluctuations be distinct from the condensate part in the definition (16). More formally, one requires the fluctuations field $\delta\Psi_n(\mathbf{k})$ to have no $n = 0, \mathbf{k} = 0$ part. The exclusion of the $\mathbf{k} = 0, n, m = 0$ part is superfluous in the tracelog term since there we have an additional sum over \mathbf{k} . The $\mathbf{k} = 0$ part would have thus no weight in the thermodynamic limit where the sum becomes an integral.

The action (18) is still exact, since the elimination of the atomic degrees of freedom could be performed exactly. Note, however, that the action contains arbitrary orders in the cavity field a_n through the logarithm and the inverse of the matrix $\mathbf{M}_{n,m}(\mathbf{k})$. The nontrivial second order contribution describes how a cavity photon gets dressed by the atoms. The higher order terms describe the interactions between photons mediated by the atoms.

A. Saddle-point equations

In the following, we will determine the complete phase diagram within a mean-field (MF) treatment. In our present problem, where direct interactions between the atoms are neglected, this saddle point approximation is in fact exact in the TL. This will be discussed in detail in section VI below. To determine the phase diagram within MF, one needs to find non-vanishing solutions of the equation(s) which correspond to extrema of the action. Specifically, we have to minimize with respect to both the cavity and condensed atoms fields

$$\frac{\partial S_{\text{eff}}[\Phi_0^\dagger, \Phi_0, a^*, a]}{\partial(a_n^*, \partial\Phi_0^\dagger)} = 0 \quad (19)$$

In addition, we need to satisfy the equation of state

$$N = \frac{1}{\mathcal{Z}} \left(\frac{\partial \mathcal{Z}}{\partial \mu} \right)_{T,V}, \quad (20)$$

which determines the average atom density $n = N/V$ as a function of the chemical potential μ .

Both the cavity and the atom field are independent of the imaginary time τ in the MF solution. The MF cavity field thus has only the zero frequency Matsubara component:

$$a_n^{\text{MF}} = \beta\delta_{n,0}\sqrt{N}\alpha. \quad (21)$$

Below the DHL transition the state of the cavity is the vacuum $\alpha = 0$, while the cavity is in a coherent state with amplitude equal to $\sqrt{N}\alpha$ above the transition.

In order to determine the full phase diagram, the values of both α and Φ_0 have to be calculated by solving the system of two coupled equations

$$\begin{cases} \mathcal{M}_\alpha(0; \mathbf{0})\Phi_0 = 0 \\ -\Delta_c\alpha + \Phi_0^\dagger \mathcal{M}'_\alpha \Phi_0 + \frac{1}{n} \sum_n \int_B \frac{d\mathbf{k}}{(2\pi)^3} \text{tr} [\mathcal{M}_\alpha^{-1}(\omega_n; \mathbf{k}) \mathcal{M}'_\alpha] = 0 \end{cases} \quad (22)$$

which arise from the saddle point condition (19). In addition, we have to satisfy the equation of state

$$\Phi_0^\dagger \Phi_0 + \frac{1}{n} \sum_n \int_{\mathcal{B}} \frac{d\mathbf{k}}{(2\pi)^3} \text{tr} [\mathcal{M}_\alpha^{-1}(\omega_n; \mathbf{k})] = 1, \quad (23)$$

obtained from (20) by evaluating the partition function in the saddle point approximation $\mathcal{Z} \simeq \exp(-S_{\text{eff}}^{\text{MF}})$. After solving these equations, the resulting MF action can be written as $S_{\text{eff}}^{\text{MF}} = \beta F_{\text{eff}}^{\text{MF}}$ where

$$F_{\text{eff}}^{\text{MF}} = -N \Delta_c |\alpha|^2 + \frac{V}{\beta} \sum_n \int_{\mathcal{B}} \frac{d\mathbf{k}}{(2\pi)^3} \text{tr} \ln [\mathcal{M}_\alpha(\omega_n; \mathbf{k})] + N \Phi_0^\dagger \frac{\mathcal{M}_\alpha(0; \mathbf{0})}{\beta} \Phi_0 \quad (24)$$

is the free energy, which is a minimum for the given values of Φ_0 and α .

In Eqs. (22),(23) and (24), we substituted the momentum sum with an integral: $\sum_{\mathbf{k} \in \mathcal{B}} \rightarrow V \int_{\mathcal{B}} d\mathbf{k}/(2\pi)^3$, and defined the MF Nambu matrix

$$\frac{1}{\beta} \mathcal{M}_\alpha(\omega_n; \mathbf{k}) = \begin{pmatrix} \dots & \dots & \dots & \dots & \dots & \dots & \dots \\ \frac{u_0}{4} |\alpha|^2 & \frac{\lambda}{2} (\alpha^* + \alpha) & \frac{1}{\beta} G_0^{-1}(\omega_n; \mathbf{k} - \mathbf{k}_0) + \frac{u_0}{2} |\alpha|^2 & \frac{\lambda}{2} (\alpha^* + \alpha) & \frac{u_0}{4} |\alpha|^2 & 0 & 0 \\ 0 & \frac{u_0}{4} |\alpha|^2 & \frac{\lambda}{2} (\alpha^* + \alpha) & \frac{1}{\beta} G_0^{-1}(\omega_n; \mathbf{k}) + \frac{u_0}{2} |\alpha|^2 & \frac{\lambda}{2} (\alpha^* + \alpha) & \frac{u_0}{4} |\alpha|^2 & 0 \\ 0 & 0 & \frac{u_0}{4} |\alpha|^2 & \frac{\lambda}{2} (\alpha^* + \alpha) & \frac{1}{\beta} G_0^{-1}(\omega_n; \mathbf{k} + \mathbf{k}_0) + \frac{u_0}{2} |\alpha|^2 & \frac{\lambda}{2} (\alpha^* + \alpha) & \frac{u_0}{4} |\alpha|^2 \\ \dots & \dots & \dots & \dots & \dots & \dots & \dots \end{pmatrix} \quad (25)$$

which is just the matrix (12) calculated for $a_n = a_n^{\text{MF}}$. Furthermore, the matrix

$$\mathcal{M}'_\alpha = \begin{pmatrix} \dots & \dots & \dots & \dots & \dots & \dots & \dots \\ \frac{u_0}{4} \alpha & \frac{\lambda}{2} & \frac{u_0}{2} \alpha & \frac{\lambda}{2} & \frac{u_0}{4} \alpha & 0 & 0 \\ 0 & \frac{u_0}{4} \alpha & \frac{\lambda}{2} & \frac{u_0}{2} \alpha & \frac{u_0}{4} \alpha & 0 & 0 \\ 0 & 0 & \frac{u_0}{4} \alpha & \frac{\lambda}{2} & \frac{u_0}{2} \alpha & \frac{\lambda}{2} & \frac{u_0}{4} \alpha \\ \dots & \dots & \dots & \dots & \dots & \dots & \dots \end{pmatrix} \quad (26)$$

is the derivative of (12) with respect to a_n^* , calculated again for $a_n = a_n^{\text{MF}}$. Note that the MF matrix $\mathcal{M}_\alpha(\omega_n; \mathbf{k})$ is diagonal in Matsubara space. This is due to the fact that in MF we have a stationary classical cavity field which has no temporal fluctuations which could couple different Matsubara sectors in the atomic field. This also implies that the last term in the action (18) does not contribute within the MF approach, since the sum is restricted to $n, m \neq 0$.

Let us briefly discuss the structure of the coupled MF equations (22). The first equation is the MF equation for the condensate spinor and actually corresponds to an infinite set of equations, one for each Bloch band (each component of Φ_0). In the numerical solution, one has to introduce a cutoff in the number of bands in the problem which also sets the size of the Nambu matrices introduced above. In order to have cutoff-independent results, the number of bands ν has to be chosen such that $\nu E_R \gg k_B T$. The second equation in (22) is the MF equation for the cavity condensate. It contains both the

coupling with the condensed atoms (second term) and to the thermal atoms (last term).

In the MF equations (22), we assumed the fields α and each component of Φ_0 to be real. The fact that the phase of both the cavity and the condensed atom field is fixed in our problem becomes evident by generalizing the real valued order parameters α and Φ_0 to include an arbitrary phase $\varphi_\alpha = \arg(\alpha)$ and $\varphi_0 = \arg(\phi_0)$. This leads to a change of the MF free energy (24) which describes Josephson like coupling terms which lock the phases of the cavity, the pump laser and the BEC together. These phase locking terms results from the two photon processes involving the pump laser (see lower diagram in Fig. 2) and are of two kinds. The first kind of Josephson term comes from the tracelog part in the free energy (24) and involves thermal atoms only. In order to understand its structure, it is useful to expand the tracelog in powers of α , resulting in

$$E_J^{\text{th}}(\alpha) = -V \frac{\lambda^2}{4} \Pi(0; \mathbf{k}_0) |\alpha|^2 \cos^2(\varphi_\alpha - \varphi_p) + O(|\alpha|^4 \cos^4(\varphi_\alpha - \varphi_p)), \quad (27)$$

where we have explicitly reintroduced the phase of the pump laser φ_p . The latter actually vanishes in the frame rotating with the pump so that the cavity phase appears alone. The function $\Pi(0; \mathbf{k}_0)$, which is defined in Eq. (30) below is positive and thus the thermal Josephson coupling E_J^{th} , which involves only even powers of $\cos(\varphi_\alpha - \varphi_p)$, is negative definite. As a result,

it is minimized whenever the phase of the cavity relative to the pump is either zero or π , corresponding to the atomic momentum distribution being peaked either at plus or minus \mathbf{k}_0 , respectively.

In the self-ordered regime below the Bose-Einstein condensation temperature, where both α and Φ_0 are non-vanishing, a further Josephson coupling arises from the last term in the free energy (24). Introducing in addition the phase $\varphi_{\mathbf{k}_0}$ of the finite momentum Fourier components of the condensate, it reads

$$E_J^{\text{BEC}}(\alpha, \Phi_0) = 4N \lambda |\alpha| |\phi_0| |\phi_{\mathbf{k}_0}| \cos(\varphi_\alpha - \varphi_p) \cos(\varphi_{\mathbf{k}_0} - \varphi_0). \quad (28)$$

For simplicity, we truncated the condensate spinor only to include $\pm \mathbf{k}_0$ components and also used the fact that the energy is minimized when the two opposite components of the condensate spinor are the same: $\phi_{-\mathbf{k}_0} = \phi_{\mathbf{k}_0}$. From Eq. (28), we see that E_J^{BEC} is minimized when the phase of the cavity field relative to the pump laser and the one of the \mathbf{k}_0 component of the condensate relative to the homogenous component are locked such that one of the two is zero and the other is π . The Josephson energy (28) thus implies a phase locking between the above relative phases as long as we have a BEC. The π -locking of the relative phase between the condensate and the cavity field is in fact analogous to what happens in an interacting BEC, where the $\mathbf{k} = 0$ condensate and the $(\mathbf{k}, -\mathbf{k})$ pairs of bosons at finite momentum \mathbf{k} are locked together by an extensive internal Josephson coupling due to the anomalous interaction terms $\sim V_k \hat{a}_k \hat{a}_{-\mathbf{k}}^\dagger \hat{a}_0^\dagger + h.c.$

Experimentally, the relative phase between the pump and the cavity field can be observed by recombining the laser beam and the photons leaking out of the cavity mirrors inside an interferometer. The $0 - \pi$ phase locking between the pump and the cavity originating from E_J^{th} has been experimentally observed both in the thermal gas [5] and in the BEC [6] self-organization. By contrast, the additional phase locking originating from E_J^{BEC} should be present only in the self ordered regime of the BEC [6], but this has not been investigated so far.

IV. SADDLE-POINT SOLUTION

We now present our results from a self-consistent numerical solution of Eqs. (22). We first present the global phase diagram, then discuss the features at the onset of spatial order, and finally describe the dynamical band structure across the phase diagram.

A. Phase diagram

Upon solving the MF equations (22), (23) for different values of the temperature T and the Rabi coupling λ we obtain the phase diagram shown in Fig. 3. It exhibits four different phases which are characterized by the two order parameters α and Φ_0 describing whether and which of the two symmetries $U(1)$, Z_2 (see section II A) of our system is broken. The

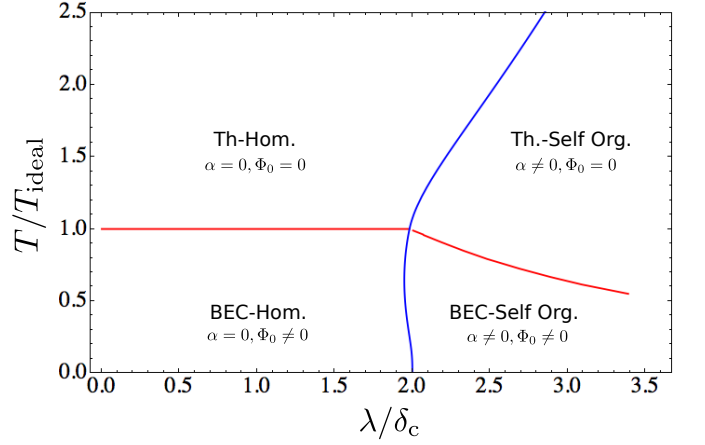


FIG. 3. Finite temperature (T) phase diagram of a Bose gas in an optical cavity as a function of atom-cavity coupling λ . The self-organization threshold λ_{so} is indicated by the blue line while the ratio of the condensation temperature T_0 to the ideal gas value T_{ideal} is indicated by red line. The crossing of these lines happens at the bi-critical point where the atoms become superfluid and spatially self-organize at the same time. Here the recoil energy $E_R = 8\delta_c$, the dispersive shift $u_0 = 0$, and the dimensionless density $\tilde{n} = 1$, where $\tilde{n} = n/(m\delta_c)^{3/2}$.

four phases are separated by the self-organization threshold λ_{so} (blue line) and the condensation temperature T_0 (red line).

The system can thus be found in i) a thermal homogeneous phase: $\alpha = 0, \Phi_0 = 0$, ii) a BEC homogeneous phase: $\alpha = 0, \Phi_0 \neq 0$ where only the continuous $U(1)$ symmetry is broken, iii) a thermal self-ordered phase: $\alpha \neq 0, \Phi_0 = 0$ where only the discrete Z_2 symmetry is broken, or iv) a self-organized BEC phase $\alpha \neq 0, \Phi_0 \neq 0$ where both symmetries are broken.

We point out that at $T = 0$ the equations (22) become equivalent to the MF equations derived with a multimode approach in [24]. In particular, at $T = 0$ we recover the value (8) of the self-organization threshold, as will be discussed in section IV B. In contrast to [24], our approach also covers the whole temperature range from the $T = 0$ BEC through the condensation temperature up to the Boltzmann gas.

In the following, we will consider in detail the main features of the phases introduced above. In section IV B we will study the self-organization threshold λ_{so} . In section IV C we will analyze the dynamical band structure appearing in the self-organized phases, giving rise to a nontrivial behavior of the condensation temperature T_0 .

B. Self-organization threshold

In the phase diagram of Fig. 3, we observe an interesting non-monotonic behavior of the self-organization threshold $\lambda_{so}(T)$ depicted as the blue line. Indeed, as the temperature increases from zero, λ_{so} decreases over a certain range of T , that is, the self-organization is favored by thermal fluctuations. This effect, which can be much more pronounced than in the example of Fig. 3, originates from the thermal occupation of the momentum continuum and will be now discussed

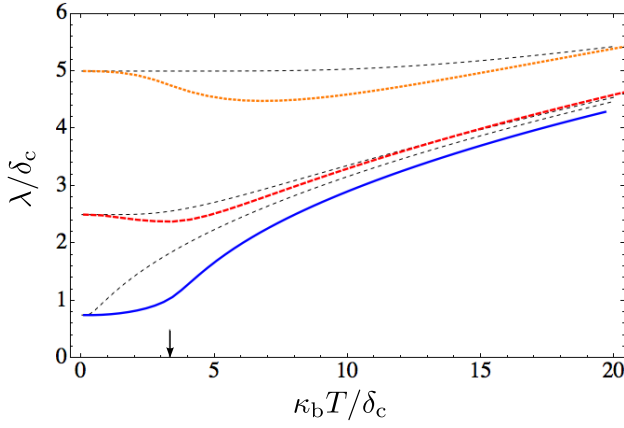


FIG. 4. The self-organization threshold λ_{so} as a function of temperature for three different values of the recoil energy: $E_R = 1.1\delta_c$ (blue solid line), $E_R = 12.5\delta_c$ (red dashed line), and $E_R = 50\delta_c$ (orange dotted line). The other parameters are $\bar{n} = 1$ and $u_0 = 0$. The black dashed lines show the correspondent prediction from the effective Dicke model λ_D . The arrow marks the value of the condensation temperature T_0 .

in detail.

It is possible to derive an analytical expression for $\lambda_{so}(T)$ by linearizing the MF equations (22) with respect to $\alpha \ll 1$. Correspondingly, one has to truncate the condensate spinor to include only the first non-zero momentum component: $\Phi_0^T = (\dots, 0, \phi(-\mathbf{k}_0), \phi(\mathbf{0}), \phi(\mathbf{k}_0), 0, \dots)$ and linearize the MF equations also with respect to $\phi(\pm\mathbf{k}_0) \ll \phi(\mathbf{0})$. By requiring the coefficient of the linear term in α in the second equation of (22) to vanish, we obtain the self-organization threshold, whose critical rescaled Rabi coupling reads

$$\lambda_{so}^2 = \frac{\delta_c}{2(n_0/n)/E_R + \Pi(0; \mathbf{k}_0)/n}, \quad (29)$$

with the bosonic Lindhard function

$$\begin{aligned} \Pi(\omega_n; \mathbf{k}) &= \frac{\beta}{V} \sum_{n_1} \sum_{\mathbf{k}_1} G_0(\omega_{n_1}; \mathbf{k}_1) G_0(\omega_n + \omega_{n_1}; \mathbf{k} + \mathbf{k}_1) \\ &= \int_{\mathcal{B}} \frac{d\mathbf{k}}{(2\pi)^3} \frac{n_b(\epsilon(\mathbf{k}) - \mu) - n_b(\epsilon(\mathbf{k} + \mathbf{k}_0) - \mu)}{\epsilon(\mathbf{k} + \mathbf{k}_0) - \epsilon(\mathbf{k}) - i\omega_n}, \end{aligned} \quad (30)$$

where $n_b(z) = (\exp(\beta z) - 1)^{-1}$ is the Bose distribution function. The Lindhard function (30) for $\mathbf{k} = \mathbf{k}_0$ essentially quantifies how important is the scattering of the cavity photons with the thermal atoms. As will be discussed in section V A, it contributes to the cavity photon self-energy. The corresponding Feynman diagram is depicted on the second line (first term) in Fig. 8. In particular, the zero frequency part is the relevant one for the self-organization threshold (29). On the other hand, the first term in the denominator of (29) corresponds to the scattering of the photon with the condensed atoms (see the second diagram on the second line in Fig. 8). Altogether, self-organization is favored by a more effective scattering between cavity photons and atoms, that is, if $2(n_0/n)/E_R + \Pi(0; \mathbf{k}_0)/n$ is increased.

In Fig. 4 $\lambda_{so}(T)$ is plotted for different values of the recoil energy E_R , and compared with the prediction of the effective

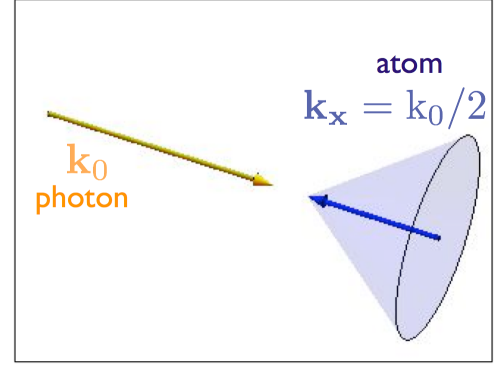


FIG. 5. Illustration of the momentum configurations of an energetically allowed scattering process between an atom and a cavity photon. The arrows three-dimensionally represent the direction and intensity of the momentum carried by the photon (yellow) and the atom (blue). The cone around the blue arrow indicates all the other possible directions of the atomic momentum giving rise to equivalent contributions to the momentum sum in $\Pi(0; \mathbf{k}_0)$

Dicke model (8). The main observation is that, given any recoil energy, the prediction of the effective Dicke model never reproduces the behavior of λ_{so} over the whole temperature range. As noted in the beginning of this section, this is due to the two main facts: i) at any finite temperature, the momentum distribution of the atoms is a continuum, and ii) the atoms can Bose condense. The first effect, dominating at large recoil (orange dotted line) affects λ_{so} through the Lindhard function. The second one, dominating for recoil energies smaller than the condensation temperature (blue solid line), enters through the temperature dependence of the condensate occupation N_0 .

The prediction of the effective Dicke model is recovered only in the very low or very high temperature regime. Indeed, if the recoil energy $E_R \gg k_B T$, we have that $\Pi(0; \mathbf{k}_0) \simeq 2(n - n_0)/E_R$ and N_0 disappears from λ_{so} . The system does not differentiate anymore between condensed and non-condensed atoms and the rescaled critical Rabi coupling becomes

$$\lambda_{so}^2 \simeq \frac{\delta_c E_R}{2} \simeq \lambda_D^2, \quad E_R \gg k_B T. \quad (31)$$

In the opposite high-temperature regime $k_B T \gg E_R, T_0$, we have instead $\Pi(0; \mathbf{k}_0) \simeq (n - n_0)/k_B T$ and $N_0 = 0$, so that the threshold becomes:

$$\lambda_{so}^2 \simeq \delta_c k_B T \simeq \lambda_D^2, \quad k_B T \gg E_R, k_B T_0. \quad (32)$$

The high-temperature behavior (32) of the critical coupling agrees precisely with the result of the semi-classical treatment of Refs. 30 and 31.

We point out that the fact that the self-organization threshold λ_{so} coincides with the Dicke model prediction (8) at high temperatures does not mean that the Dicke model correctly describes the system in this regime. In fact, the atomic momentum distribution is a continuum and cannot be truncated to contain only $\mathbf{k} = 0$ and $\pm\mathbf{k} + 0$. This does not show up in

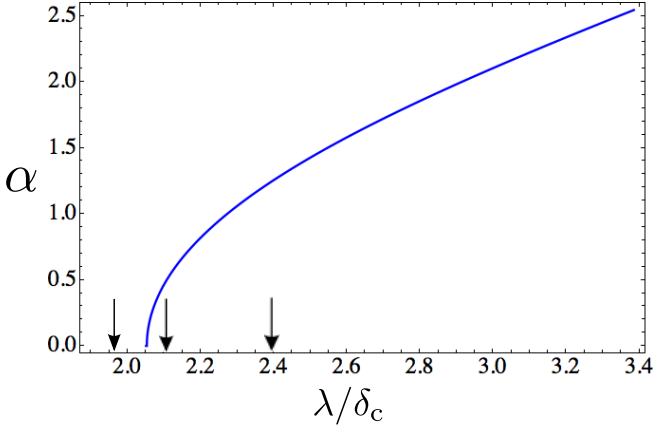


FIG. 6. Onset of the coherent cavity condensate α as a function of the Rabi coupling λ at a given temperature $k_B T = 4\delta_c > T_0$. The parameters are the same as in Fig. 3.

the result for λ_{so} because the latter depends only on the zero-frequency part of the Lindhard function, which for $k_B T \gg E_R$ does not depend anymore on the recoil energy.

In order to experimentally probe both these limiting temperature regimes, and in particular the intermediate regime where novel features beyond the Dicke model appear, one would need to prepare the system at different temperatures both below and above the recoil energy. This should be possible with cold atoms where typically both the critical temperature scale $k_B T_0$ and the recoil energy E_R are in the KHz range.

An interesting novel feature that we observe is the existence of an optimal temperature for which $\lambda_{so}(T)$ is minimum. This feature, already noticeable in the phase diagram of Fig. 3, becomes more pronounced for recoil energies large compared to $k_B T_0$, as apparent from Fig. 4. As anticipated in the beginning of this section, the existence of a minimum for $\lambda_{so}(T)$ is an effect of thermal occupation of the momentum continuum and is due to the fact that, over a certain range of temperature, $\Pi(0; \mathbf{k}_0)$ grows with T .

Let us consider the Lindhard function as written on the second line of (30) and put $\omega_n = 0$. For the present argument, the relevant contribution to the momentum integral is coming from momenta such that the denominator is zero. There is no singularity since the numerator is also zero, yielding a finite value. This corresponds to an event where the atom has the same energy before and after scattering with the photon (see again section V A). This happens every time that the scattering takes place in the configuration illustrated in Fig. 5. The only condition to be fulfilled in order for the atom not to change its energy in the scattering is that its momentum component along the cavity direction is equal to half of the photon momentum: $k_x = -k_0/2$. This means that a whole continuum of momenta satisfying this condition, indicated by the blue cone in Fig. 5, give a large contribution to the momentum integral in (30). With increasing the temperature, this continuum of momenta which differ only in their component transverse to the cavity axis, acquires a larger occupation with the net effect of increasing $\Pi(0; \mathbf{k}_0)$ and thus decreasing λ_{so} .

However, as can be seen in Fig. 4, when T becomes com-

parable or larger than $\epsilon(\mathbf{k}_0/2) = E_R/4$, the temperature starts to disfavor the self-organization. This is due to the occupation of larger momenta along the cavity direction which subtracts weight from the $k_x \sim -k_0/2$ region.

We thus understand the minimum in $\lambda_{so}(T)$ as resulting from the competition between the smearing out of the occupation of the $k_0/2$ momentum state along the cavity direction and the occupation of the continuum of momentum states transverse to the cavity direction.

It is interesting to note that an analogous effect of temperature on self-organization has been numerically observed also for a different setup, where the atoms are trapped inside a two-dimensional lattice and interacting with a cavity mode [39].

C. Dynamical band structure

An example of the behavior of the cavity condensate α across the self-organization transition is shown in Fig. 6. In this example the system is above the condensation temperature $T > T_0$ so that $\Phi_0 = 0$. After the threshold $\lambda_{so} = 2.05\delta_c$ the cavity MF α grows like $\sqrt{1 - (\lambda/\lambda_{so})^2}$, giving rise to a lattice felt by the atoms. This lattice has a wavevector \mathbf{k}_0 with corresponding amplitude $V_{\mathbf{k}_0} = \lambda\alpha$, and a wavevector $2\mathbf{k}_0$ with amplitude $V_{2\mathbf{k}_0} = u_0\alpha^2/4$. These amplitudes may be viewed as “dynamical” since they depend on α which in turn depends on the atomic configuration.

The corresponding band structure is shown in Fig. 7. We see that, as soon as we cross the self-organization threshold λ_{so} , band gaps appear due to a nonzero lattice depth. The size of the band gaps increases monotonically with the distance from the critical coupling. In the example of Fig. 7, the tight binding regime is reached already for $\lambda = 1.2\lambda_{so}$ (right panel).

The band structure $E(\mathbf{k})$ is obtained by finding the poles of the matrix $\mathcal{M}_\alpha^{-1}(-i\omega; \mathbf{k})$ for the real frequency ω , which amounts to finding the eigenvalues of $\mathcal{M}_\alpha(0; \mathbf{k})$. In general, we have one pole for each Bloch band. Having found the poles, we can evaluate the Matsubara sums in the Eqs. (22). In particular, the equation of state becomes:

$$N = N_0 + \sum_{\mathbf{k} \in \mathcal{B}} \sum_{\nu} n_b(E_\nu(\mathbf{k})), \quad (33)$$

where ν is a positive integer labelling the different Bloch bands. We note that $N_0 = 0$ in the example of Fig. 7.

The fact that the lattice is dynamical becomes apparent by examining the equation of state (33) together with the second MF equation (22) (assume for simplicity that we have no condensed atoms $N_0 = 0$). At given N, V, T and also λ, u_0 , the value of α fixes the band structure $E_\nu(\mathbf{k})$ which, through Eq. (33), determines how the atoms occupy the different bands. The resulting chemical potential enters the second equation in (22), determining the amplitude α of the cavity mode. This feedback loop implies that the band structure here is quite different from the rigid band structure in optical lattices [33]: it depends on how the atoms occupy the bands.

An important consequence of having a dynamical band structure is that the lattice depth at a given λ depends on temperature. The condensation temperature T_0 must be thus

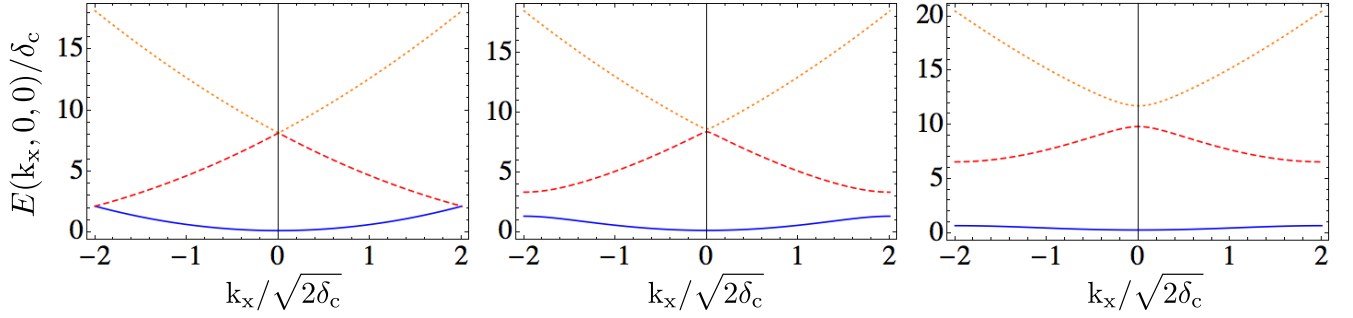


FIG. 7. Dynamical band structure across the self-organization transition (from left to right) displaying the opening of band gaps induced by the coherent cavity field. The three panels show the low band structure for three different values of λ , marked by the arrows in Fig. 6. The parameters are the same as in Fig. 6.

self-consistently determined and is not directly obtained from λ . An example behavior of T_0 is depicted in Fig. 3 (red line). Outside the self-organized phase $\lambda < \lambda_{so}$, the MF equation of state is the same as the one of an ideal homogeneous Bose gas, and thus T_0 takes the corresponding value $T_{ideal} = 3.31(N/V)^{2/3}/mk_B$ independent of λ . In section V we will show that this actually holds in general (not only in the MF approximation) in the TL. In the self-organized phase instead, due to the presence of a lattice, T_0 starts decreasing with λ . The depth of the lattice is indeed a monotonic function of λ and a decreasing behavior is thus qualitatively expected.

V. PHOTON DYNAMICS AROUND SADDLE-POINT

In this section, we compute the cavity spectrum and study its temperature dependence across the condensation temperature, as well as its behavior close to the DHL self-organization transition. We will restrict our analysis to the homogeneous phase $\lambda < \lambda_{so}$. In this phase, the cavity coherent field $\alpha = 0$ and the atomic condensate is homogeneous $\Phi_0^T = (\dots, 0, \sqrt{N_0/N}, 0, \dots)$.

A. Photon self-energy

In this subsection, we derive the renormalized cavity photon propagator from which we compute the spectral function in the following subsection.

Since $\alpha = 0$, we can expand the action (18) in the cavity field a_n . Up to second order, the effective action reads (see appendix A for details of the derivation)

$$S_{\text{eff}}^{(2)}[a^*, a] = -\beta\mu N_0 + \sum_n \sum_{\mathbf{k}} \ln(G_0^{-1}(\omega_n; \mathbf{k})) + \frac{1}{2\beta^2} \sum_n \begin{pmatrix} a_n^* & a_{-n} \end{pmatrix} \mathcal{G}^{-1}(\omega_n) \begin{pmatrix} a_n \\ a_{-n}^* \end{pmatrix}, \quad (34)$$

where the inverse cavity propagator reads:

$$\mathcal{G}^{-1}(\omega_n)/\beta = \begin{pmatrix} -i\omega_n - \Delta_c + \Sigma_{u_0} + \Sigma(\omega_n) & \Sigma(\omega_n) \\ \Sigma(\omega_n) & i\omega_n - \Delta_c + \Sigma_{u_0} + \Sigma(\omega_n) \end{pmatrix}, \quad (35)$$

with the two kinds of self-energies:

$$\Sigma_{u_0} = \frac{1}{2}u_0 \quad (36)$$

$$\Sigma(\omega_n) = -\lambda^2 \left[\frac{1}{2n} \Pi(\omega_n; \mathbf{k}_0) + \frac{(n_0/n)E_R}{\omega_n^2 + E_R^2} \right]. \quad (37)$$

The first self-energy, whose corresponding Feynman diagrams are shown on the first line in Fig. 8, results from events without momentum transfer between the photon and the atoms. These correspond to Hartree-terms proportional to the average single-atom dispersive shift u_0 . We have one single internal atomic line proportional to $G_0(\omega_s; \mathbf{k})$ for thermal atoms or proportional to N_0 for condensed atoms. For thermal atoms, upon performing the internal loop frequency and momentum sum, we obtain simply $n - n_0$ and thus the two contributions to Σ_{u_0} in Fig. 8 sum up to yield an overall dispersive shift, as given in Eq. (36).

The second self-energy (37) involves events where the photon transfers momentum \mathbf{k}_0 either to a thermal atom (first term on the second line in Fig. 8) or to a condensed atom (second term on the second line in Fig. 8). As anticipated in section IV B, the former diagram corresponds to the Lindhard function defined in Eq. (30) for $\mathbf{k} = \mathbf{k}_0$. Indeed, we have two internal lines for thermal atoms each proportional to G_0 but with

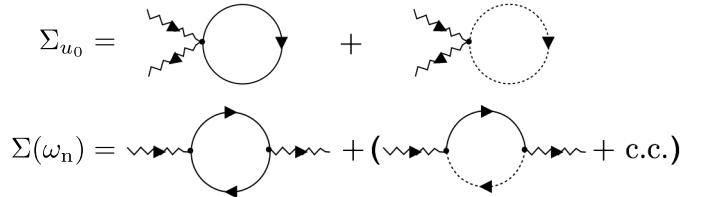


FIG. 8. Feynman diagrams contributing to the photon self-energy. The zig-zag lines are for photons, the straight solid lines for thermal atoms, and the dashed lines for condensed atoms.

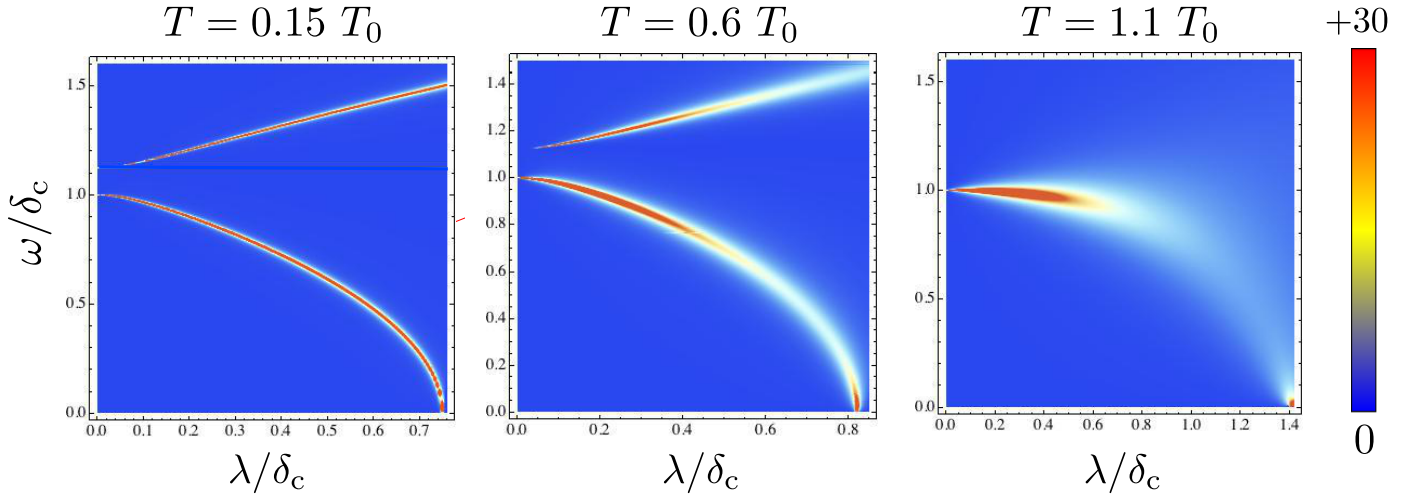


FIG. 9. Behavior of the photon spectral function with increasing temperature. The two-dimensional color plots show $A(\omega)$ as a function of the coupling λ for different values of the temperature. Here the condensation temperature is $T_0 = 3.31\delta_c$ and the recoil energy is $E_R = 1.125\delta_c$. Also $u_0 = 0$ and $\tilde{n} = 1$.

frequency and momentum differing by the photon frequency ω_n and the photon momentum \mathbf{k}_0 . Finally, the second term on the second line in Fig. 8 contains a thermal atomic line G_0 with the same frequency and momentum as the photon, and also a condensed line proportional to N_0 . This diagram is imaginary and sums up with its complex conjugate to yield N_0 times the real part of G_0 , as given in the second term of Eq. (37).

From the propagator (35) we can immediately derive the expression (29) for the self-organization threshold λ_{so} by requiring that $\text{Det}[\mathcal{G}^{-1}(0)] = 0$. This amounts to requiring the existence of a zero frequency mode in the excitation spectrum, i. e. a soft mode. The properties of the spectrum will be discussed in detail in section V B by means of the spectral function.

Although in the following we will always use the general form of the self-energies given in Eqs. (36) and (37), it is interesting to look at their behavior in the limiting regime of large recoil energy $E_R \gg k_B T$. In this case, the Lindhard function simplifies to $\Pi(\omega_n; \mathbf{k}_0) \simeq 2(n - n_0)E_R/(\omega_n^2 + E_R^2)$ and sums up with the condensed atom contribution in the self-energy (37), to yield $\Sigma(\omega_n) \simeq -\lambda^2 E_R/(\omega_n^2 + E_R^2)$, which does not depend on the condensate occupation N_0 anymore. As noted also in section IV B, this means that in this regime the system does not differentiate between condensed and non-condensed atoms and we recover the physics of two-level atoms with the effective resonance E_R .

B. Cavity spectral function

We now want to study the spectral function of our effective cavity below the self-organization transition. From the cavity propagator defined in Eq. (35), we obtain the spectral function

$$\mathcal{A}(\omega) = 2\text{Im}\mathcal{G}(-i\omega + 0^+) \quad (38)$$

by analytic continuation. We will here discuss the diagonal element of the two by two matrix $\mathcal{A}(\omega)$, namely:

$$A(\omega) = \frac{-2(\delta_c + \omega)^2 \text{Im}\Sigma(-i\omega + 0^+)}{[\delta_c^2 - \omega^2 + 2\delta_c \text{Re}\Sigma(-i\omega + 0^+)]^2 + [2\delta_c \text{Im}\Sigma(-i\omega + 0^+)]^2}, \quad (39)$$

which corresponds to the analytical continuation of the normal propagator $G_{11}(\tau) = \langle T \hat{a}(\tau) \hat{a}^\dagger \rangle$, where T is the time ordering operator. The spectral function $A(\omega)$ describes how the spectral weight of the bare cavity mode is split and broadened by the coupling with the atoms through the driving laser field. As done in the experiment [8], this can be probed by exciting the cavity with a weak pulse.

Typical examples of $A(\omega)$ as a function of the coupling λ are

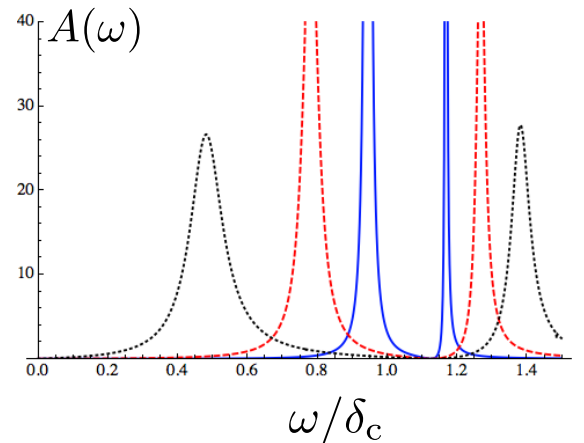


FIG. 10. The spectral function for the case $T = 0.6T_0$ at fixed $\lambda = 0.17\delta_c, 0.41\delta_c, 0.67\delta_c$ for the blue-solid, red-dashed, and black-dotted line, respectively.

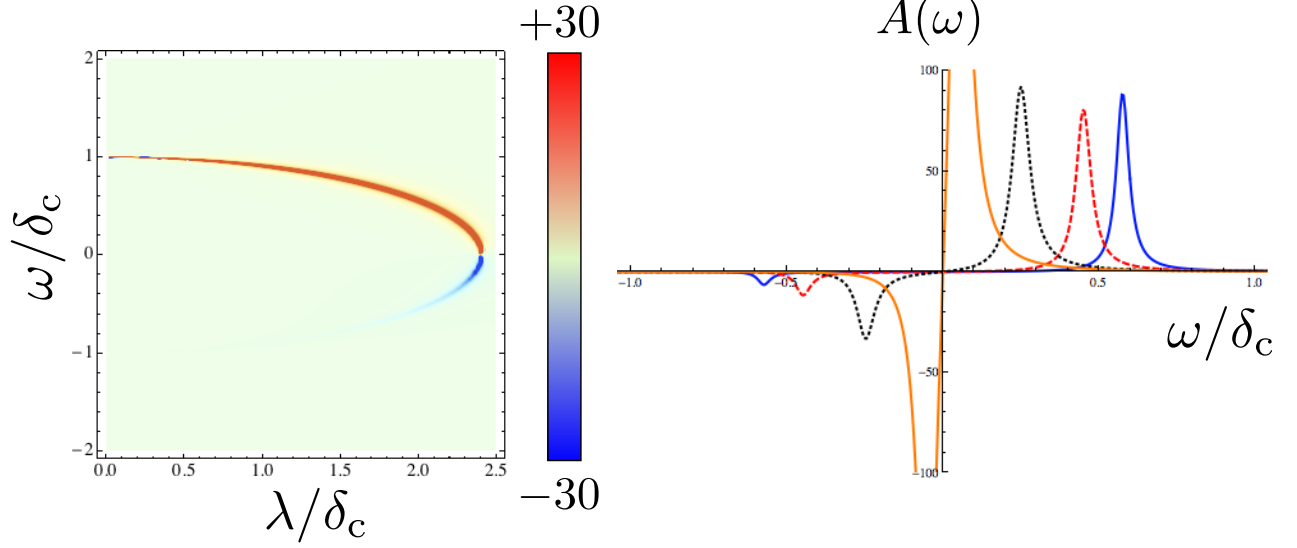


FIG. 11. Behavior of the spectral function towards the self-organization transition. The two-dimensional colour plot shows $A(\omega)$ as a function of the coupling λ . The right panel shows the spectral function for at fixed $\lambda = 1.97\delta_c, 2.15\delta_c, 2.33\delta_c, 2.40\delta_c$ for the blue-solid, red-dashed, black-dotted line, and orange solid line respectively. Here the recoil energy is $E_R = 12.5\delta_c$ and $T = 4\delta_c$. Also $u_0 = 0$ and $\tilde{n} = 1$.

given in Fig. 9 and 10. In general, we observe two peaks corresponding to the two polaritonic branches: the atomic branch, starting from the value $\omega = E_R$ for $\lambda = 0$ with zero spectral weight, and the photonic branch, starting as a delta-peak at the value δ_c for $\lambda = 0$. The peak corresponding to the lowest branch (the photonic one in the figures) is then shifted towards $\omega = 0$ as λ increases and reaches zero at λ_{so} . This mode softening, which has been demonstrated experimentally [8], has some interesting features that we will discuss at the end of this section.

Let us start by considering the effect of temperature plus the momentum continuum on the spectral function. In all the examples presented in Fig. 9 we have a broadening of the polaritonic peaks, which is also evident by looking at the spectral function at given λ , as shown in Fig. 10. The broadening is induced by the coupling of the cavity with thermal atoms such that a polariton can decay by exchanging momentum and energy with the latter. Formally, this is due to the fact that the analytic continuation yields an imaginary part to the self-energy $\Sigma(-i\omega + 0^+)$ through the Lindhard function (30). Indeed we have:

$$\text{Im}\Pi(-i\omega + 0^+; \mathbf{k}_0) = \frac{\beta\pi^3}{\ell_T^4 k_0} \ln \left[\frac{e^{\beta\left(\frac{|\omega - E_R|^2}{4E_R} - \mu\right)} - e^{-\beta\omega}}{e^{\beta\left(\frac{|\omega - E_R|^2}{4E_R} - \mu\right)} - 1} \right], \quad (40)$$

where $\ell_T = 2\pi/\sqrt{2mk_B T}$ is the thermal wavelength. From eq. (40), we see that the imaginary part vanishes for $T = 0$. In general, for $k_0\ell_T \gg 1$, the broadening is strongly suppressed, as can be seen in the left panel of Fig. 9. This is consistent with the previously observed fact that in this regime we recover the physics of two-level atoms for an effective Dicke model, which indeed should have no broadening of the polaritonic peaks in absence of dissipation. Upon increasing the

temperature the broadening increases especially on the upper polaritonic branch. In particular, by comparing the $T = 0.6T_0$ with the $T = 1.1T_0$ case in Fig. 9, we can observe the effect of crossing the condensation temperature T_0 . The upper polariton peak gets quickly washed out and a strongly broadened lower polariton peak remains. This is due to the vanishing of the condensate N_0 . The latter contributes to the spectral function with a sharp feature since the corresponding self-energy (second term in Eq. (37)), has no imaginary part. However, the upper polaritonic branch is not strictly a signature of the presence of the atomic condensate. This is true only when the polariton energy is much smaller than $k_B T_0$, as in the example of Fig. 9. Indeed, in this regime the broadening due to the coupling with thermal atoms close to T_0 is so large that, without a condensate, the upper branch will be completely washed away. On the other hand, if we choose δ_c and the recoil E_R much larger than the temperature, the latter has no such effect on the polaritons, as long as we stay far enough from the transition. For instance, even at large temperatures, we recover the usual collective Rabi splitting, whereby the two equally broadened polaritonic peaks move apart for increasing (and small enough) coupling.

In Fig. 9 and 10, we see that the broadening increases with the coupling λ . However, close enough to the self-organization threshold, the soft mode peak seems to become well defined again. This feature is mostly evident in the right-most panel of Fig. 9, where the soft mode peak first is washed out but then reappears very close to the transition. As we shall discuss now, the peak is not actually becoming sharper, but acquiring a diverging weight.

Let us analyze the behavior of the spectral function close to the transition in more detail with the help of Fig. 11. Here the negative frequency part of $A(\omega)$ is also shown. Close

enough to the transition, a well defined peak with negative spectral weight appears at negative frequency. This negative peak compensates the weight coming from the positive peak thereby enforcing the sum rule $\int_{-\infty}^{+\infty} d\omega A(\omega) = 2\pi$. This negative frequency branch corresponds to excitations where the cavity extracts photons from the pump laser through the interaction via the atoms. Indeed, the coupling with the laser gives rise to terms proportional to $a + a^*$ in the effective action (10) after integrating out the excited atomic state. This term in turn produce anomalous components in the propagator (35) even in absence of the cavity condensate, yielding negative frequency modes with negative spectral weight.

The closer we get to the transition, the stronger becomes the negative peak which also moves towards zero frequency in a symmetric way with respect to the positive frequency part. Close to λ_{so} and for small ω , we can derive an analytical expression for the spectral function:

$$A(\omega) \simeq \frac{C(T)\omega}{\left[\delta_c^2 \left(1 - \left(\frac{\lambda}{\lambda_{so}} \right)^2 \right) - 2 \left(1 - \left(\frac{\lambda}{\lambda_{so}} \right)^2 \right) \omega^2 \right] + (C(T)\omega)^2}, \quad (41)$$

where $C(T) = \beta^2 \lambda_{so}^2 (\pi^3 / \ell_T^4 n k_0) n_b (\epsilon(\mathbf{k}_0/2) - \mu)$. The above expression illustrates the $1/\omega$ behavior for $\lambda \rightarrow \lambda_{so}$, noticeable in the right panel of Fig. 11. This can be physically interpreted as a situation in which the cavity can extract photons from the pump laser with perfect efficiency, which is indeed what should happen at the self-organization transition.

In the denominator of the spectral function (38), the first term between square brackets determines the position of the peak in the spectral function, while the last term sets the width of the peak according to the broadening factor $C(T)$. However, as we see from Eq. (41), this interpretation is not valid for the soft mode at the transition, since the term setting the width has the same ω -dependence as the one responsible for the peak position. This is due to the fact that the peak broadening, proportional to the imaginary part of the self energy (40), behaves like ω at small frequency. This implies that the polaritons are not well defined quasiparticles for $\omega \rightarrow 0$. Further insight into this aspect is provided by analyzing the behavior of the poles of the propagator $\mathcal{G}(-i\omega + 0^+)$. These are determined by the equation: $\delta_c^2 - \omega^2 + 2\delta_c \Sigma = 0$. The result for the soft mode pole is:

$$\omega_- \simeq \frac{\delta_c}{2} \left(\sqrt{1 - \left(\frac{\lambda}{\lambda_{so}} \right)^2 - C^2(T)} - iC(T) \right). \quad (42)$$

Far enough from the transition, the term under the square root is positive therefore the pole has both an imaginary part, related to the broadening factor $C(T)$, and a real part. However, close enough to the transition, the term in the square root must become negative, thereby making the soft mode pole purely imaginary

$$\omega_- \simeq \frac{-i}{C(T)} \frac{\lambda_{so} - \lambda}{\lambda_{so}}. \quad (43)$$

This means that the soft mode becomes overdamped close to the transition with the position of the pole vanishing linearly with $\lambda_{so} - \lambda$ along the imaginary axis. This behavior is the

same, but the origin of the effect different, as observed in [28] in a calculation of the two-state Dicke model with photon decay. In that reference, the broadening and overdamping of the polariton excitations is due to coupling of photons to the bath of electromagnetic modes outside the cavity. In the present paper, the polaritons become dissipative from coupling to the thermal bath of bosonic atoms.

The behavior (41) of the spectral function close to the transition determines the photon flux exponent [18, 27, 28] characterizing the divergence of the average photon density at the critical point. Indeed, at thermal equilibrium the following relation holds [40]: $\langle \hat{a}^\dagger \hat{a} \rangle = G_{11}(0^-) = \int \frac{d\omega}{2\pi} A(\omega) n_b(\omega)$. Since the divergence comes from the small frequency part of the integral, we can approximate $n_b(\omega) \simeq 1/\beta\omega$ and perform the integral in an interval around $\omega = 0$ using the expression (41), to get:

$$\langle \hat{a}^\dagger \hat{a} \rangle \propto (\lambda - \lambda_{so})^{-1}, \quad (44)$$

which gives a photon flux exponent equal to one, typical of a thermal behavior. The same exponent was also found in [28], where the thermal character of the steady state was again to “thermal” noise from cavity decay. The result (44) is valid at any finite temperature. At $T = 0$ instead, since $A(\omega) \propto \delta(\omega - \omega_-)$, we have $\langle \hat{a}^\dagger \hat{a} \rangle \propto 1/\omega_- \propto (\lambda - \lambda_{so})^{-1/2}$ as expected [25, 27, 28].

VI. MEAN-FIELD NATURE OF THE SELF-ORGANIZATION TRANSITION

In this section, we study the scaling of the fluctuations in the TL and show that the self-organization transition is of the MF type. Indeed, as we will show below, the corrections to the MF solution in the self-organized phase vanish in the TL, and in the homogeneous phase the Gaussian theory for the fluctuations about the cavity vacuum, corresponding to the action (34), becomes exact. Moreover, we will show that there is no quantum depletion of the atomic condensate in absence of additional short-range interactions between the atoms.

Up to now, we have truncated our expansion of the action (18) around the cavity MF at the second order in the cavity fluctuations to obtain the action (34). However, higher order terms, corresponding to interactions between the cavity photons mediated by the atoms, can in principle be relevant. For instance, in the framework of an effective Ginzburg-Landau theory for the cavity field, the higher order terms are needed to determine the nature of our self-ordering transition. In this section, we will study the full effective action (18) in the TL, where some exact statements can be made.

Let us consider the scaling in the TL of the diagrams appearing in our theory. For instance, consider a typical self-energy diagram, like the one in Fig. 8. Since for each photonic leg we have a vertex scaling like $1/\sqrt{N}$, such a diagram scales like unity for the fluctuations $\omega_n \neq 0$ and like N for the MF (when the external photonic legs are proportional to $\sqrt{N}\alpha$). Indeed, there is no external loop thus no scaling from the external legs, apart from the MF diagrams. The same reasoning can be applied to a typical interaction (4-th order) term, like

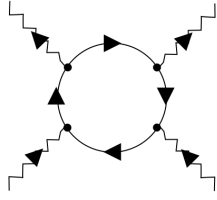


FIG. 12. Typical 4-th order Feynman diagram describing the atom-mediated interaction between cavity photons. The notation is the same as in Fig. 8.

the one in Fig. 12. In this case, the addition of two external legs brings a further $1/N$ scaling due to the vertices, but no further scaling due to the external lines, apart again from the MF diagrams. Therefore, a typical 4-th order diagram scales like $1/N$ for the fluctuations and like N for the MF.

These scaling arguments have several important implications: First, the MF diagrams contribute to all orders in the cavity field, i.e. the action (24) cannot be truncated at some power of α . Moreover, the fluctuation diagrams, at most of order one, are negligible with respect to the MF diagrams $\propto V$. Therefore, the MF approach discussed in section IV becomes exact in the TL. This is the same as it happens for the restricted BCS model [41, 42] where the coupling between fermions takes place only at fixed exchanged momentum equal to zero. We will come again to this analogy at the end of this section. In all our calculations, we found that our MF approach predicts a continuous self-organization transition.

Clearly, outside the self-organized phase the MF $\alpha = 0$ and we are left with the fluctuation diagrams only. Yet, we are allowed to retain only the self-energy diagrams of Fig. 8 and neglect all the interaction diagrams which scale like $1/N$. This means that the action (34) becomes exact in the TL and we have a free Gaussian theory. This in turn implies that the cavity propagator (35) becomes exact in the TL.

A further relevant implication of the above scaling arguments is that the fluctuations originating from the cavity do not deplete the atomic condensate in the TL. This is due again to the fact that these fluctuations are of order unity and are thus negligible with respect to the number of atoms N . In particular, since the cavity fluctuations are the only quantum fluctuations (surviving even at $T = 0$), we conclude that there is no quantum depletion of the atomic condensate in the TL.

We point out that the scaling arguments also apply if one includes short-range interactions between the atoms. More precisely, the fact that the mean-field is exact in the TL still holds, even though the model is not exactly solvable anymore. The underlying reason for these scalings is the fact that the cavity photons have only one fixed momentum. That is, we have one single degree of freedom $a(\tau)$ in zero dimensions. In this sense, the self-organization transition is to be regarded as a quantum bifurcation rather than a quantum phase transition. Indeed, there is no divergent length scale and no quantum critical behavior, like it happens in the standard Dicke model.

The exactness of MF theory for the present problem can be understood from a different point of view by considering the effective interaction between atoms which is mediated by

the cavity photons. This interaction is obtained from the full action (10) by integrating out the cavity field a_n . Since the latter only appears quadratically, this is a Gaussian integration which can formally be done at the expense of introducing terms beyond quadratic order in the ground state atomic field $\psi_{n,k}$. Expanding the resulting action up to fourth order in $\psi_{n,k}$, one obtains a standard density-density interaction between the atoms of the form

$$S_{\text{int}} = -\frac{\lambda^2}{2N} \times \int_{-\beta/2}^{\beta/2} d\tau d\tau' \int_V d\mathbf{r} d\mathbf{r}' n(\tau, \mathbf{r}) \cos(\mathbf{k}_0 \cdot \mathbf{r}) \mathcal{G}(\tau - \tau') \cos(\mathbf{k}_0 \cdot \mathbf{r}') n(\tau', \mathbf{r}'), \quad (45)$$

where $n(\tau, \mathbf{r}) = \psi^\dagger(\tau, \mathbf{r})\psi(\tau, \mathbf{r})$ is the atom density. The interaction is retarded on a scale which is set by the real part of the photon propagator

$$\mathcal{G}(\tau) = \frac{\cosh[-\Delta_c(\beta/2 - |\tau|)]}{\sinh[-\Delta_c\beta/2]}. \quad (46)$$

In the limit of a large and negative detuning $|\Delta_c| \gg k_B T$, $\Delta_c < 0$ this retardation is negligible, however, because $|\Delta_c| \mathcal{G}(\tau) \rightarrow \delta(\tau)$. We recall that to arrive at Eq. (45), we also took the detuning atom-pump detuning Δ_a , typically in the GHz regime, to be much larger than the recoil energy and the atomic chemical potential, typically in the KHz regime. In that regime, we can also safely discard potential retardation effects arising from propagation of the intermediate excited state in the 2-photon processes described earlier in Fig. 2. The effective interaction Hamiltonian which is associated with the action (45) can be written in the form

$$\hat{H}_{\text{int}} = -\frac{\lambda^2}{2N|\Delta_c|} \hat{\rho}_{\mathbf{k}_0} \hat{\rho}_{\mathbf{k}_0}, \quad (47)$$

where $\hat{\rho}_{\mathbf{k}_0} = \int_V d\mathbf{r} \hat{\psi}^\dagger(\mathbf{r}) \hat{\psi}(\mathbf{r}) \cos(\mathbf{k}_0 \cdot \mathbf{r})$ is the Fourier transform of the atom density at wave vectors $\pm \mathbf{k}_0$.

Remarkably, the above interaction term Eq. (45) is of the same form than the interaction term in the reduced BCS model of attractively interacting fermions upon replacing $\hat{\rho}_{\mathbf{k}_0} \hat{\rho}_{\mathbf{k}_0}$ with $\hat{B}_0^\dagger \hat{B}_0$, where $\hat{B}_0 = \int_V d\mathbf{r} \hat{\psi}_\uparrow(\mathbf{r}) \hat{\psi}_\downarrow(\mathbf{r})$ is the total number of zero momentum fermion bilinears. In a classic paper [41], Mühlischlegel has shown that such reduced models are solved exactly within mean-field theory (see also Ref. 43). Diagrammatically, this means that the exact free energy density consists of all connected “bubble” diagrams in each of which the prefactor $1/N$ cancels with the loop integration over all degrees of freedom. Higher-order corrections from inserting additional vertices and closing external legs (for example of the type shown in Fig. 12), will generate additional vertices each scaling as $1/N$. Because the momentum-transfer at each vertex is restricted to exactly equal \mathbf{k}_0 here, or zero in the BCS model, these vanish.

Note that for the DHL self-organization transition, the order parameter is a real-valued density wave (dual to the coherent cavity field appearing in Eq. (24)), whereas in the BCS model the order parameter is in general a complex-valued Cooper

pairing amplitude. Condensation of Cooper pairs breaks a $U(1)$ symmetry because the operator B_0 may have an arbitrary phase, while in our case $\hat{\rho}_{\mathbf{k}_0}$ is real and the only remaining degeneracy is the discrete parity, which corresponds to ordering in $+\mathbf{k}_0$ or $-\mathbf{k}_0$, a Z_2 symmetry (see Ref. 44 for an explanation of an analogous Z_2 -type mean-field model for commensurate charge ordering of fermions in a half-filled hypercubic lattice).

VII. CONCLUSIONS

This paper provided an exact solution of the interplay of Bose-Einstein condensation (BEC) and the Dicke-Hepp-Lieb (DHL) self-organization transition of a Bose gas at arbitrary temperatures subject to a dynamical optical potential generated by the electromagnetic vacuum field of a high-quality optical resonator.

We showed that, at finite temperatures, the typically invoked Hilbert space truncation to only two atomic momentum states, that leads to a description in terms of a zero-dimensional effective Dicke model, becomes unphysical and breaks down. We developed an effective action approach that captures the dynamical multi-band structure, that the cavity generates for the atoms, as well as the backaction of the atoms on the cavity spectrum. Using this approach, we computed the full phase diagram at arbitrary temperature and discovered a bi-critical point, at which the atoms become superfluid and self-organize at the same time. We showed that the thermally excitable continuum of atomic finite momentum states can enhance self-organization in striking contrast to the finite-temperature solution of the Dicke model where a finite temperature always counteracts ferromagnetic spin order. Moreover, the thermal bath of atoms strongly broadens and overdamps the polaritonic sidebands of the cavity spectrum.

We also gained some structural insights and argued that the cavity-Bose gas problem, in the absence of short-range interactions between the atoms, belongs to a class of exactly solvable, so called restricted, mean-field models, the most prominent of which is the celebrated BCS-theory of superconductivity. It is remarkable that many-body cavity QED provides a natural, experimental incarnation of such models. We note that also the experimentally relevant non-equilibrium extensions of the model of this paper, that is, coupling the photons and atoms to Markovian baths, will remain exactly solvable as long as potential loss and gain terms are operative on the single-particle level.

Our calculations were carried out in a frame rotating with the optical frequency of the driving laser. In that frame, the periodically driven Bose gas in a cavity can be formulated as a time-independent Hamiltonian problem. We here employed an equilibrium path integral formalism without explicitly accounting for the finite photon lifetimes and spontaneous emission of the atoms. This means we have implicitly assumed a dissipative loss channel for the energy deposited by the drive laser without accounting for the usually arising noise terms (from the fluctuation-dissipation theorem). This approach is not rigorous but has been shown to work well for the unitary (reversible) sector of the non-equilibrium steady states for

Dicke-type models in cavity QED (see e.g. Ref. 22, 28, and 45 for detailed comparison between the equilibrium and non-equilibrium steady states). In particular the phase diagram and basic features of the spectral properties only receive relatively small, quantitative modifications from the dissipation. The fact that the Markovian baths typical of quantum optics generate a finite, effective temperature at long times further supports the usage of an equilibrium formalism. In the present context, the main aspect that the equilibrium formalism misses are (additional) imaginary contributions to the poles of correlation functions which should lead to irreversible, overdamped dynamics especially close to the self-organization transition. The equilibrium formalism also is not able to differentiate between the transient regimes at shorter times, which should be the most relevant for a refined comparison with experiments, and the asymptotic long-time regimes, which have so far been the focus of most of the theoretical works.

In the future, it will be interesting to generalize the results obtained in the present paper to lossy cavities and clarify further the dissipative effects induced by a finite temperature versus those induced by cavity decay. It should also be possible to consider interacting Bose gases in a cavity and study the competition of cavity-mediated interaction, short-range repulsion, and dissipation in the superfluid regime.

ACKNOWLEDGMENTS

We thank Mikhail D. Lukin, Steffen P. Rath, and Richard Schmidt for helpful discussions and gratefully acknowledge useful remarks on the manuscript by Michael Buchhold and Sarang Gopalakrishnan. F. P. acknowledges support from the Alexander Von Humboldt foundation. The research of PS was supported by the DFG under grant Str 1176/1-1, by the NSF under Grant DMR-1103860, by the Army Research Office Award W911NF-12-1-0227, by the Center for Ultracold Atoms (CUA) and by the Multidisciplinary University Research Initiative (MURI).

Appendix A: Derivation of the photon propagator

Our goal in this appendix is to derive the action (34) from the full effective action (18) by expanding the latter to second order in the cavity field a_n . To this purpose, we write the Nambu matrix (12) as:

$$\mathbf{M}_{n,m}(\mathbf{k}) = \delta_{n,m} G_0^{-1}(\omega_n; \mathbf{k}) + \mathbf{Q}_{n,m}, \quad (\text{A1})$$

where the matrix $G_0^{-1}(\omega_n; \mathbf{k})$ is diagonal in Nambu space with elements $(\dots, G_0^{-1}(\omega_n; \mathbf{k} - \mathbf{k}_0), G_0^{-1}(\omega_n; \mathbf{k}), G_0^{-1}(\omega_n; \mathbf{k} + \mathbf{k}_0), \dots)$, and the matrix

$$\mathbf{Q}_{n,m} = \begin{pmatrix} \dots & \dots & \dots \\ U_{n,m} & \Lambda_{n,m}/2 & U_{n,m}/2 \\ \Lambda_{n,m}/2 & U_{n,m} & \Lambda_{n,m}/2 \\ U_{n,m}/2 & \Lambda_{n,m}/2 & U_{n,m} \\ \dots & \dots & \dots \end{pmatrix}. \quad (\text{A2})$$

We then expand the tracelog and the inverse as follows:

$$\begin{aligned} \text{Tr} \ln (\mathbb{I}_n G_0^{-1} + Q) &= \\ \text{Tr} \ln (\mathbb{I}_n G_0^{-1}) + \text{Tr} (\mathbb{I}_n G_0 Q) - \frac{1}{2} \text{Tr} [(\mathbb{I}_n G_0 Q)^2] + \dots, \\ (\mathbb{I}_n G_0^{-1} + Q)^{-1} &= \\ \mathbb{I}_n G_0 - \mathbb{I}_n G_0 Q \mathbb{I}_n G_0 + (\mathbb{I}_n G_0 Q)^2 \mathbb{I}_n G_0 + \dots, \end{aligned} \quad (\text{A3})$$

where \mathbb{I}_n is the identity matrix in Matsubara space. As an example, let us consider the term:

$$\begin{aligned} \text{Tr} \ln (\mathbb{I}_n G_0^{-1}) &= \sum_n \sum_{\mathbf{k} \in B} \left[\dots + \ln (G_0^{-1}(\omega_n; \mathbf{k} - \mathbf{k}_0)) + \ln (G_0^{-1}(\omega_n; \mathbf{k})) + \ln (G_0^{-1}(\omega_n; \mathbf{k} + \mathbf{k}_0)) + \dots \right] = \\ &= \sum_n \sum_{\mathbf{k}} \ln (G_0^{-1}(\omega_n; \mathbf{k})) . \end{aligned} \quad (\text{A4})$$

For the last equality, we have transformed a sum of terms each with a momentum sum restricted to the first Brillouin zone into a single term with an unrestricted momentum sum. With

analogous manipulations we can also obtain:

$$\begin{aligned} \text{Tr} (\mathbb{I}_n G_0 Q) &= \frac{u_0}{2N\beta} \sum_n |a_n|^2 \sum_{\mathbf{n}_1, \mathbf{k}} G_0(\omega_{\mathbf{n}_1}; \mathbf{k}) \\ &= \frac{u_0(1 - N_0/N)}{2\beta} \sum_n |a_n|^2, \end{aligned} \quad (\text{A5})$$

up to second order in a_n . For the last equality we have used the fact, as discussed in section VI, that the ideal gas equation of state is exact in the TL whereby $\sum_{\mathbf{n}, \mathbf{k}} G_0(\omega_{\mathbf{n}}; \mathbf{k}) = N - N_0$. Up to second order in a_n , the last contribution we get from the tracelog comes from:

$$\begin{aligned} &-\frac{1}{2} \text{Tr} [(\mathbb{I}_n G_0 Q)^2] = \\ &-\frac{1}{2} \sum_{n, m} \sum_{\mathbf{k} \in B} \frac{\Lambda_{n, m} \Lambda_{m, n}}{2} [\dots + G_0(\omega_n; \mathbf{k}) G_0(\omega_m; \mathbf{k} - \mathbf{k}_0) + G_0(\omega_n; \mathbf{k}) G_0(\omega_m; \mathbf{k} + \mathbf{k}_0) + \\ &+ G_0(\omega_n; \mathbf{k} - \mathbf{k}_0) G_0(\omega_m; \mathbf{k}) + G_0(\omega_n; \mathbf{k} + \mathbf{k}_0) G_0(\omega_m; \mathbf{k}) + \dots] = \\ &-\frac{\lambda^2}{2n} \sum_n \frac{1}{2} \Pi(\omega_n; \mathbf{k}_0) (a_n^* a_n + a_{-n}^* a_{-n} + a_n^* a_{-n}^* + a_n a_{-n}) . \end{aligned} \quad (\text{A6})$$

The above contribution corresponds to the first term in the self-energy (37).

Let us now turn to the expansion of the last term of the action (18). The only second order contribution comes from

the first term in the expansion of M^{-1} given above. Taking into account that the condensate spinor is simply $\Phi_0^T = (\dots, 0, \sqrt{N_0/N}, 0, \dots)$, this second order contribution reads:

$$\begin{aligned}
& -N \sum_{n,m \neq 0} \Phi_0^\dagger M_{0,n}(\mathbf{0}) \delta_{n,m} G_0(\omega_n; \mathbf{k}) M_{m,0}(\mathbf{0}) \Phi_0 = \\
& = -N_0 \sum_{n \neq 0} \frac{\Lambda_{n,0} \Lambda_{0,n}}{4} (G_0(\omega_n; -\mathbf{k}_0) + G_0(\omega_n; \mathbf{k}_0)) = -\frac{\lambda^2 N_0 / N}{2\beta} \sum_{n \neq 0} \frac{E_R}{\omega_n^2 + E_R^2} (a_n^* a_n + a_{-n}^* a_{-n} + a_n^* a_{-n}^* + a_n a_{-n}) . \quad (A7)
\end{aligned}$$

For the last equality we used the fact that $\Lambda_{n,0} \Lambda_{0,n} = \Lambda_{-n,0} \Lambda_{0,-n}$ in order to sum the propagator $G_0(\omega_n; \mathbf{k}_0)$ with its complex conjugate. The above contribution corresponds to the second term in the self-energy (37). The first term on the second line in Eq. (18) can be written as

$$N \Phi_0^\dagger M_{0,0}(\mathbf{0}) \Phi_0 = -\mu \beta N_0 + \frac{1}{2} u_0 (N_0 / N) \frac{1}{\beta} \sum_n |a_n|^2 . \quad (A8)$$

The last term above sums up with the Eq. (A5) to yield the self-energy (36).

-
- [1] S. Haroche, and J. M. Raimond, *Exploring the Quantum: Atoms, Cavities, and Photons*, Oxford University Press (2006)
 - [2] S. Gleyzes, *et al.*, Nature **446**, 297 (2007)
 - [3] R. J. Thompson, G. Rempe, and H. J. Kimble, Phys. Rev. Lett. **68**, 1132 (1992)
 - [4] P. Domokos, and H. Ritsch, Phys. Rev. Lett. **89**, 253003 (2002)
 - [5] A. T. Black, H. W. Chan, and V. Vuletić, Phys. Rev. Lett. **91**, 203001 (2003)
 - [6] K. Baumann, C. Guerlin, F. Brennecke, and T. Esslinger, Nature **464**, 1301 (2010)
 - [7] K. Baumann, R. Mottl, F. Brennecke, and T. Esslinger Phys. Rev. Lett. **107**, 140402 (2011)
 - [8] R. Mottl, *et al.*, Science **336**, 1570 (2012)
 - [9] F. Brennecke, *et al.*, arXiv:1304.4939v1
 - [10] S. Inouye, *et al.*, Science **285**, 571 (1999)
 - [11] Y. Yoshikawa, Y. Torii, and T. Kuga, Phys. Rev. Lett. **94**, 083602 (2005)
 - [12] S. Slama, *et al.*, Phys. Rev. Lett. **98**, 053603 (2007)
 - [13] R. Bonifacio, and L. De Salvo, Nucl. Instrum. Methods **341**, 360 (1994)
 - [14] R. H. Dicke, Phys. Rev. **93**, 99 (1954)
 - [15] H. Ritsch, P. Domokos, F. Brennecke, and T. Esslinger, Rev. Mod. Phys. **85**, 553 (2013)
 - [16] A. Vukics, C. Maschler, and H. Ritsch, New J. Phys. **9**, 255 (2007)
 - [17] F. Dimer, *et al.*, Phys. Rev. A **75**, 013804 (2007)
 - [18] D. Nagy, G. Szirmai, and P. Domokos, EPJD **48**, 127 (2008)
 - [19] J. Larson, and M. Lewenstein, NJP **11**, 063027 (2009)
 - [20] D. Nagy, G. Konya, G. Szirmai, and P. Domokos, Phys. Rev. Lett. **104**, 130401 (2010)
 - [21] J. Keeling, M.J. Bhaseen, B.D. Simons, Phys. Rev. Lett. **105**, 043001 (2010)
 - [22] S. Gopalakrishnan, B. L. Lev, and P. M. Goldbart, Phys. Rev. A **82**, 043612 (2010)
 - [23] S.F. Vidal, G. De Chiara, J. Larson, G. Morigi, Phys. Rev. A **81**, 043407 (2010)
 - [24] G. Konya, G. Szirmai, and P. Domokos, EPJD **65**, 33 (2011)
 - [25] D. Nagy, G. Szirmai, and P. Domokos, Phys. Rev. A **84**, 043637 (2011)
 - [26] M. J. Bhaseen, J. Mayoh, B. D. Simons, and J. Keeling, Phys. Rev. A **85**, 013817 (2012)
 - [27] B. Öztóp, M. Bordyuh, O. E. Müstecaplıoglu, and H. E. Türeci, New J. Phys. **14**, 085011 (2012)
 - [28] E. G. Dalla Torre, *et al.*, Phys. Rev. A **87**, 023831 (2012)
 - [29] D. E. Chang, J. I. Cirac, and H. J. Kimble, Phys. Rev. Lett. **110**, 113606 (2013)
 - [30] J.K. Asbóth, P. Domokos, H. Ritsch, and A. Vukics, Phys. Rev. A **72**, 053417 (2005)
 - [31] D. Nagy, J. K. Asbóth, P. Domokos, and H. Ritsch, Europhys. Lett. **74**, 254 (2006)
 - [32] C. Maschler, I. Mekhov, and H. Ritsch, EPJD **46**, 545 (2008)
 - [33] I. Bloch, J. Dalibard and W. Zwerger, Rev. Mod. Phys. **80**, 885 (2008)
 - [34] C. Emary and T. Brandes, Phys. Rev. E **67**, 066203 (2003)
 - [35] J. Ye, and C. Zhang, Phys. Rev. A **84**, 023840 (2011)
 - [36] K. Hepp, and E. H. Lieb, Ann. of Phys. **76**, 360 (1973)
 - [37] Y. K. Wang, and F. T. Hioe, Phys. Rev. A **7**, 831 (1973)
 - [38] N. Lambert, C. Emary, and T. Brandes, Phys. Rev. Lett. **92**, 073602 (2004)
 - [39] Y.-Q. Li, L. He, and W. Hofstetter, arXiv:1205.0813
 - [40] A. Altland, and B. Simons, *Condensed Matter Field Theory*, Cambridge Univ. Press (2010)
 - [41] B. Mühlischlegel, J. Math. Phys. **3**, 522 (1962)
 - [42] J. Dukelsy, S. Pittel, and G. Sierra, Rev. Mod. Phys. **76**, 643 (2004)
 - [43] R. Haag, Il Nuovo Cimento **25**, 287 (1962)
 - [44] R. Gersch, C. Honerkamp, D. Rohe, and W. Metzner, Eur. Phys. J. B **48**, 349 (2005)
 - [45] M. Buchhold, P. Strack, S. Sachdev, and S. Diehl, arXiv:1304.5196 (2013)